NASA/TM—2005-213384

High Speed Civil Transport (HSCT) Isolated Nacelle Transonic Boattail Drag Study and Results Using Computational Fluid Dynamics (CFD)

Anthony C. Midea
Glenn Research Center, Cleveland, Ohio

Thomas Austin
McDonnell Douglas Aerospace, Long Beach, California

S. Paul Pao
Langley Research Center, Hampton, Virginia

James R. DeBonis
Glenn Research Center, Cleveland, Ohio

Mori Mani
McDonnell Douglas Aerospace, St. Louis, Missouri

February 2005

The NASA STI Program Office . . . in Profile

Since its founding, NASA has been dedicated to the advancement of aeronautics and space science. The NASA Scientific and Technical Information (STI) Program Office plays a key part in helping NASA maintain this important role.

The NASA STI Program Office is operated by Langley Research Center, the Lead Center for NASA's scientific and technical information. The NASA STI Program Office provides access to the NASA STI Database, the largest collection of aeronautical and space science STI in the world. The Program Office is also NASA's institutional mechanism for disseminating the results of its research and development activities. These results are published by NASA in the NASA STI Report Series, which includes the following report types:

- TECHNICAL PUBLICATION. Reports of completed research or a major significant phase of research that present the results of NASA programs and include extensive data or theoretical analysis. Includes compilations of significant scientific and technical data and information deemed to be of continuing reference value. NASA's counterpart of peer-reviewed formal professional papers but has less stringent limitations on manuscript length and extent of graphic presentations.

- TECHNICAL MEMORANDUM. Scientific and technical findings that are preliminary or of specialized interest, e.g., quick release reports, working papers, and bibliographies that contain minimal annotation. Does not contain extensive analysis.

- CONTRACTOR REPORT. Scientific and technical findings by NASA-sponsored contractors and grantees.

- CONFERENCE PUBLICATION. Collected papers from scientific and technical conferences, symposia, seminars, or other meetings sponsored or cosponsored by NASA.

- SPECIAL PUBLICATION. Scientific, technical, or historical information from NASA programs, projects, and missions, often concerned with subjects having substantial public interest.

- TECHNICAL TRANSLATION. English-language translations of foreign scientific and technical material pertinent to NASA's mission.

Specialized services that complement the STI Program Office's diverse offerings include creating custom thesauri, building customized databases, organizing and publishing research results . . . even providing videos.

For more information about the NASA STI Program Office, see the following:

- Access the NASA STI Program Home Page at ***http://www.sti.nasa.gov***

- E-mail your question via the Internet to help@sti.nasa.gov

- Fax your question to the NASA Access Help Desk at 301–621–0134

- Telephone the NASA Access Help Desk at 301–621–0390

- Write to:
  NASA Access Help Desk
  NASA Center for AeroSpace Information
  7121 Standard Drive
  Hanover, MD 21076

NASA/TM—2005-213384

High Speed Civil Transport (HSCT) Isolated Nacelle Transonic Boattail Drag Study and Results Using Computational Fluid Dynamics (CFD)

Anthony C. Midea
Glenn Research Center, Cleveland, Ohio

Thomas Austin
McDonnell Douglas Aerospace, Long Beach, California

S. Paul Pao
Langley Research Center, Hampton, Virginia

James R. DeBonis
Glenn Research Center, Cleveland, Ohio

Mori Mani
McDonnell Douglas Aerospace, St. Louis, Missouri

National Aeronautics and
Space Administration

Glenn Research Center

February 2005

Acknowledgments

The authors wish to thank the following team members for their dedicated effort. The success of this study is directly related to the excellent quality of the results generated by the following personnel; Nick Geogiadis, Fred Smith, and Joe Holcomb, NASA Glenn Research Center; Khaled Abdol-Hamid, John Carlson, and Peter Coen, NASA Langley Research Center; and Ray Cosner, Chris Culbertson, Greg Finfrock, Jay Jones, Rob Jonietz, Walt LaBozzetta, Bill Regnier, and Hoyt Wallace, McDonnell Douglas Aerospace.

Document History

This research was originally published internally as HSR025 in February 1996.

Note that at the time of writing, the NASA Lewis Research Center
was undergoing a name change to the
NASA John H. Glenn Research Center at Lewis Field.
Both names may appear in this report.

Available from

NASA Center for Aerospace Information
7121 Standard Drive
Hanover, MD 21076

National Technical Information Service
5285 Port Royal Road
Springfield, VA 22100

Available electronically at http://gltrs.grc.nasa.gov

High Speed Civil Transport (HSCT) Isolated Nacelle Transonic Boattail Drag Study and Results Using Computational Fluid Dynamics (CFD)

Anthony C. Midea
NASA Lewis Research Center
Cleveland, OH 44135

Thomas Austin
McDonnell Douglas Aerospace
Long Beach, CA 90807

S. Paul Pao
NASA Langley Research Center
Hampton, VA 23681

James R. DeBonis
NASA Lewis Research Center
Cleveland, OH 44135

Mori Mani
McDonnell Douglas Aerospace
St. Louis, MO 63166

ABSTRACT

Nozzle boattail drag is significant for the High Speed Civil Transport (HSCT) and can be as high as 25% of the overall propulsion system thrust at transonic conditions. Thus, nozzle boattail drag has the potential to create a thrust-drag pinch and can reduce HSCT aircraft aerodynamic efficiencies at transonic operating conditions. In order to accurately predict HSCT performance, it is imperative that nozzle boattail drag be accurately predicted.

Previous methods to predict HSCT nozzle boattail drag were suspect in the transonic regime. In addition, previous prediction methods were unable to account for complex nozzle geometry and were not flexible enough for engine cycle trade studies. A computational fluid dynamics (CFD) effort was conducted by NASA and McDonnell Douglas to evaluate the magnitude and characteristics of HSCT nozzle boattail drag at transonic conditions. A team of engineers used various CFD codes and provided consistent, accurate boattail drag coefficient predictions for a family of HSCT nozzle configurations. The CFD results were incorporated into a nozzle drag database that encompassed the entire HSCT flight regime and provided the basis for an accurate and flexible prediction methodology.

INTRODUCTION

Nozzle boattail drag is caused by the generation of shock wave systems and regions of boundary layer flow separation on the nozzle external boattail surfaces. The shock wave systems and flow separation are due to the effects of the local flow field over the nacelle afterbody geometric curvature, and these effects yield a peak in nozzle boattail drag coefficient

at transonic conditions. For the High Speed Civil Transport (HSCT), nozzle boattail drag is significant in the transonic flight regime, and can be as high as 25% of the overall propulsion system thrust. Thus, nozzle boattail drag has the potential to create a thrust-drag pinch and can reduce HSCT aircraft aerodynamic efficiencies at transonic operating conditions (Mach 0.95 to Mach 1.1). HSCT vehicle sizing and mission performance can be significantly impacted by transonic nozzle boattail drag predictions. In order to accurately predict HSCT performance, it is imperative that nozzle boattail drag be accurately predicted.

Background

Prior to March 1995, HSCT nozzle boattail drag was predicted using an equivalent axisymmetric area method. This method was formulated by NASA and industry and assumed that nozzle geometry could be approximated with simple area ratio and length data. For axisymmetric nozzles, the method was based on an empirical axisymmetric nozzle database, (Silhan & Cubbage data, ref. 1). Plots of nozzle boattail drag as a function of Mach number were made from these test data for constant area ratio with boattail flap angle as the independent variable. Figure 1 shows an example of one of these plots at constant nozzle area ratio of 0.5. Similar plots exist for area ratios of 0.1, 0.25, 0.75 and 1.0. Nozzle length ratio was defined as nozzle exit height (h_9) divided by maximum nozzle external area height (h_{10}), or h_9/h_{10}. Nozzle area ratio was defined as nozzle exit area (A_9) divided by maximum nozzle external area (A_{10}), or A_9/A_{10}. Boattail flap angle (β) was calculated using A_9, A_{10} and the divergent flap external length between A_9 and A_{10}. Nozzle boattail drag was then determined using the five empirical tables and the following inputs; (Mach number, A_9/A_{10} and β).

For non-axisymmetric (e.g. 2D) nozzles, the tables were updated, but the method of calculating boattail angle remained the same. In effect, the non-axisymmetric nozzle boattail angle was calculated assuming equivalent axisymmetric areas. The tables of empirical axisymmetric data were updated to represent non-axisymmetric nozzles using drag deltas between axisymmetric and non-axisymmetric nozzle types obtained from a parametric linear theory analysis. This approximation was adequate for the preliminary design phase of the HSCT project, but proved to be inadequate for detailed nozzle design studies.

Much of the HSCT propulsion system activity focused on non-axisymmetric nozzles. Detailed design studies of non-axisymmetric nozzles exposed various deficiencies with the previous boattail drag method. The original axisymmetric database yielded little transonic drag information, and the curves were approximated from Mach 0.9 to 1.1. Typically, boattail drag coefficient peaks in this Mach regime at all altitudes, thus, it was possible that the peak boattail drag coefficients and transonic drag rise characteristics were not being approximated correctly. This deficiency translated from the axisymmetric drag table to the non-axisymmetric drag table approximations as well. In fact, Figure 2 shows a comparison of the previous non-axisymmetric method with experimental boattail drag data for a non-axisymmetric nozzle (ref. 2). This comparison shows that the previous method significantly underpredicted the transonic boattail drag coefficient for this specific nozzle configuration. Comparisons of the previous method with various non-axisymmetric nozzle drag coefficient experimental data were made, and the results were consistent with the trends shown in Figure 2.

The previous boattail drag method used a simple method to approximate nozzle geometry that ignored nozzle boattail sidewalls, radius of curvature (RC/RCM), 3-D effects and other detailed design characteristics. In effect, the method was too simple to differentiate between a family of detailed nozzle designs. For example, Figure 3 shows a comparison between the previous non-axisymmetric method with experimental boattail drag data for a non-axisymmetric nozzle (ref. 3). This comparison shows that the previous non-axisymmetric method cannot accurately approximate nozzle boattail drag trends due to detailed design geometry changes, such as changes in nozzle radius of curvature ratio (RC/RCM). Nozzle radius of curvature ratio is essentially a measure of the smoothness of the area distribution of the nozzle. A RC/RCM=0.0 indicates a nozzle with a sharp angle at the boattail flap hinge line. A

RC/RCM=1.0 indicates a nozzle with no discontinous wall surface slope changes from the nozzle maximum area to the nozzle exit. Because of its inability to characterize detailed nozzle geometry changes, the previous method was not flexible enough to conduct engine cycle and nozzle trade studies that are required to differentiate between detailed nozzle designs and perform component downselect activities.

In summary, the previous nozzle boattail drag prediction methodology for non-axisymmetric nozzles was not accurate in the transonic flight regime, and was not flexible enough to capture the effects on boattail drag due to detailed three-dimensional geometry changes. A new method was required to accurately predict boattail drag in a timely fashion throughout the flight regime.

Approach

Based on previous experience, transonic nozzle drag data would be difficult to obtain. The approach taken to achieve the above goal was to employ advanced Navier-Stokes computational fluid dynamics (CFD) methods to obtain accurate and reliable transonic nozzle drag coefficient data. In addition, a concurrent activity was initiated to implement an Integral Mean Slope (IMS) method using an updated nozzle boattail drag coefficient database to predict boattail drag. The IMS method is widely used and offers a detailed representation of nozzle geometry in a timely fashion (ref. 4). The nozzle boattail drag database was to be updated for the entire flight regime using all known wind tunnel and flight test data for HSCT type nozzles. The results of the nozzle drag database update are discussed in ref. 5. The transonic CFD boattail drag coefficient predictions were to be used to update and substantiate the IMS transonic nozzle boattail drag coefficient database. The following paragraphs discuss the approach and results of the CFD effort to update and substantiate the transonic nozzle drag database for the HSCT project.

METHOD OF ANALYSIS

The goal of the CFD study was to generate transonic boattail drag data for HSCT specific non-axisymmetric nozzles operating in the Mach 0.95 to 1.2 range. A family of nozzles was to be studied, and the absolute boattail drag coefficients, as well as the delta drag coefficients between specific nozzles, were to be recorded and used to validate and update the IMS database.

Four teams of analysts were involved in the CFD study; NASA Lewis Research Center - LeRC (Propulsion Systems Division, Aerospace Analysis Office), NASA Langley Research Center - LaRC (Component Integration Branch), McDonnell Douglas Aerospace - Advanced Transport Aircraft Development (ATAD) and New Aircraft and Missile Products (NAMP). Each team participated in the study with unique flow solvers as described below. In addition, all work was funded internally by each of the participating teams, respectively.

Flow Solvers

The NASA LeRC CFD flow solver was NPARC, which is a general purpose Navier-Stokes CFD solver used extensively for propulsion system flow simulations. The code is supported by the NPARC Alliance, which is made up of NASA LeRC and the U.S. Air Force Arnold Engineering Development Center, and is discussed in detail in ref. 6. NPARC solved Reynolds averaged Navier-Stokes equations in conservation law form using the Beam-Warming approximate factorization scheme. Several options were available for modeling turbulence ranging from algebraic to two-equation transport models. For this study, a one-equation Baldwin-Barth turbulence model was used based upon the results from the validation study, which will be discussed in detail later. NPARC was very flexible in handling computational grids. The user was allowed to specify a boundary condition on any portion of a grid surface. In addition, the

code allowed for complex geometry to be handled using one grid block or multiple grid blocks. However, overlap between blocks was required for interpolation of the flow quantities.

The NASA LaRC CFD flow solver was PAB3D, which is a general Navier-Stokes CFD solver developed at LaRC (ref. 7). The code architecture allowed for multiple flow solvers and boundary conditions selected by the user. The code was modular and had a multi-block structure with directionally selected grid sequencing. In addition, the code had compact memory requirements and is compatible with most workstations. The flow solver used mixed Roe and Van Leer schemes for solution accuracy and fast convergence. For this study, a two equation, k-ε turbulence model was used based on the results of the validation study. This model had also been validated for attached, shear and separated flow applications. This code operated very quickly, and only requires 38 microseconds (Cray-Ymp) per iteration per grid point. The grid sensitivity was automatically verified by grid sequencing.

The McDonnell Douglas Aerospace flow solver was NASTD, which is a general Navier-Stokes CFD flow solver developed at McDonnell Douglas (ref. 8). This code is the main CFD numerical simulation platform used at McDonnell Douglas. NASTD worked on structured (patched and overlapping) and unstructured grids, and could compute the flow field over extremely complex aerospace vehicle configurations. The code employed multiple numerical algorithms, including upwind and central difference methods. NASTD allowed use of multiple turbulence models, but a one-equation, Spalart-Allmaras turbulence model was used for this study based on the results of the validation study. The one-equation Spalart-Allmaras turbulence model was similar to the one-equation Baldwin-Barth turbulence model used with NPARC for this study. The code operated on most computer platforms, and had low memory requirements. In addition, NASTD implemented Parallel Virtual Machine (PVM) to provide distributed workstation parallel processing.

Code Validation Approach

Three unique flow solvers were used in this study, and the first step in the approach was to validate these unique flow solvers for a representative configuration. Prior to this study, PAB3D and NASTD were validated for axisymmetric and non-axisymmetric nozzles in the transonic Mach number regime. This work was done for the Advisory Group for Aerospace Research and Development (AGARD) Working Group #17 (ref. 9). Computations of pressure coefficient for axisymmetric nozzles with and without flow separation, and non-axisymmetric nozzles with flow separation were validated with experimental data. The results can be found in refs. 7, 9, 10 and 11 for PAB3D and ref. 9 for NASTD. NPARC had not yet been validated using the AGARD Working Group #17 data. Therefore, NASA LeRC was required to validate NPARC prior to participating in this CFD study. The AGARD data was acquired from MDA, and NPARC was executed for the various configurations. NPARC results compared favorably with the AGARD data (ref. 12) and, thus, NPARC was validated and approved for use in this study. Details of the comparisons of NPARC, PAB3D and NASTD to the non-axisymmetric AGARD nozzle data will be summarized later.

After all of the codes were successfully validated, the team effort focused on HSCT specific configurations. In order to ensure accuracy of results between codes, a baseline case was selected from the matrix of nozzles to be studied. This baseline case, which is described below, was evaluated by all four teams for Mach 0.95, 1.1 and 1.2 conditions. It was required that results from the four teams for the baseline nozzle agreed within a small error band (at a given Mach number) prior to commencing the entire CFD study. Comparison of team results for the baseline case will be discussed later.

Configuration Definition

Figure 4 shows a typical isolated HSCT nacelle configuration used in the CFD study. The general configuration characteristics are given here. The inlet was modeled as a generic,

axisymmetric inlet with a mass flow ratio of 1.0 (no spillage). Also, the upstream inviscid streamtube was modeled. The nozzle geometry was based on the HSCT non-axisymmetric nozzle design (Downstream Mixer (DSM) mixer/ejector nozzle). The nozzle geometry was scaled to the full scale mixed flow turbofan (MFTF) size, which is described below. The nozzle sidewalls were modeled, and the corners of the nozzle were rounded with 8 inch radii to match the DSM design. The nozzle was designed with a sharp transition at the external flap hinge line, thus representing a radius of curvature ratio (RC/RCM) of zero. Internally, the nozzle plenum chamber, throat, diffuser and exit were modeled, and the nozzle internal flow was modeled with hot gas. The internal nozzle angle was fixed at 1.5 degrees to maintain a constant exit flow divergence angle.

A family of nozzles was studied at three freestream Mach numbers; M=0.95, 1.1 and 1.2. Various nozzle boattail angle and nozzle height ratio values were modeled to represent a wide array of nozzle configurations. Boattail angles of 12, 16 and 20 degrees were chosen to encompass the range of boattail angles expected at transonic conditions. Also, nozzle height ratios of 0.2 and 0.5 were chosen to encompass the range of height ratios expected at transonic conditions. These height ratios correspond to nozzle area ratios of 0.187 and 0.467, respectively. The matrix of nozzle configurations studied is described below.

At the time of this study, the 3765-100 MFTF was the leading engine cycle candidate. This cycle was a mixed flow turbofan, designed by Pratt & Whitney and General Electric, and had a fan pressure ratio of 3.7, and required 900 lb/s of corrected airflow at sea level static conditions. For this cycle, the cycle required airflow at cruise was 65% of the required takeoff airflow. The airflow lapse rate was simply the percentage of cycle flow at cruise versus takeoff conditions. This cycle had a bypass ratio of 0.622, and had demonstrated feasible HSCT aircraft performance. Area and pressure data were obtained from the engine company datapack to define the nozzle plenum conditions, (e.g. throat area, pressure, temperature, etc.). Therefore, the hot gas flow should closely approximate the actual 3765 MFTF cycle installed with a DSM type nozzle.

The inlet, engine cycle and nozzle components were integrated, and a nacelle shape was chosen. The nacelle shape was axisymmetric at the inlet cowl lip, and continuously transitioned from axisymmetric to non-axisymmetric ending at a non-axisymmetric (2D) shape at the external flap hinge line. From the hinge line aft to the nozzle exit, the nozzle was non-axisymmetric (2D). The nacelle was modeled full scale and was based on the 3765-100 airflow requirements. This study only examined the isolated nacelle, and did not explore the effects of integrating the nacelle with a wing. Therefore, wing effects were not modeled. One-quarter of the nacelle was actually modeled with the CFD grid, and horizontal and vertical streamwise symmetry were assumed. This saved considerable computational resources with no loss in accuracy of results.

The configuration run matrix is shown in Figure 5. The N1605 configuration was the baseline configuration that was studied by all four teams. The 16 in the configuration designation represented the boattail angle in degrees, and the 05 represents a height ratio of 0.5. Each team was responsible for the N1605 configuration and one other configuration. Because each configuration was to be run at three Mach numbers (0.95, 1.1, and 1.2), this represented a total of 6 CFD runs per team member. NASA LaRC was also responsible for the N0010 configuration, which contributed three additional CFD runs and were critical for the purposes of this study. The N0010 configuration represented a nozzle with zero boattail angle, and a height ratio of 1.0. In this study, only the pressure drag due to the nozzle boattail surfaces were of interest. Thus, the pressure drag of the N0010 nacelle was subtracted from the pressure drag of all the other CFD runs (at the respective Mach number) to obtain the nozzle boattail pressure drag at any given condition.

Figure 6 shows a typical nacelle grid for a full nacelle and a side view of a representative quarter nacelle complete with the internal and external nozzle characteristics. All grid topologies and initial grids were defined by MDA for this study. NASA LaRC optimized the final surface and

volume grids for use by all teams. The grids were 3D, structured, patched, viscous, multi-block grids. The external and internal surfaces were modeled as viscous surfaces, and a viscous grid was generated to model free shear layers in the nozzle exhaust. The nozzle sidewall trailing edge was modeled with zero thickness, and the sidewalls ended at the trailing edge of the external flaps. All zones were point-matched except for upstream and far-field zones. The nozzle plenum chamber configuration was based on the AGARD non-axisymmetric nozzle configuration. A total of approximately 1.5 million grid points were used for each individual configuration. A non-dimensional viscous height of $y^+ = 2$ was employed to define the first grid cell spacing off the viscous surfaces.

The CFD flow type definition ground rules for each configuration are shown in Figure 7. An Euler region was defined just prior to the nacelle configuration to simulate the captured streamtube, and a small laminar region was defined at the nacelle leading edge to simulate transition. The problems were set up in this fashion to allow the flow solvers to begin the solution free of discontinuities. The remaining nacelle was modeled as a turbulent region.

The CFD convergence criteria were as follows. The boattail pressure drag force level required convergence within 0.1% of the total drag force. In addition, the internal nozzle exit massflow rate level required convergence within 0.25% of the intake massflow rate, (e.g. conservation of mass). Finally, the L2 residuals required reduction in the boattail flap region by three orders of magnitude. All three criteria were required to be met as a condition for a converged solution.

Nozzle boattail drag was computed using the predicted pressure distributions on the boattail surfaces. Integration of the pressure distributions over the respective nozzle boattail surfaces yielded the nozzle boattail drag results. The surfaces used in the integration included the nozzle flaps and nozzle sidewalls. Skin friction drag was not computed. Because the nozzle boattail drag for each of the configurations was influenced by the presence of the nacelle forward of the nacelle maximum area, the reference nacelle drag (configuration N0010) was subtracted from the actual boattail drag for each configuration. The reference nacelle had zero boattail angle. The results from these computations are discussed in detail later.

DISCUSSION OF RESULTS

Consistency and accuracy were the paramount concern for the success of this CFD effort. Consistency of configurations, grid topographies, and other factors was required to ensure consistency of results. A significant amount of effort was expended to ensure that the same grids were used by all team members, and that the methods used by each team were comparable.

Although the methods and groundrules for all the teams were the same, each code was still required to prove it could generate accurate results for isolated, non-axisymmetric nozzle, external surface, viscous fluid flow problems. The first step in this code validation process involved comparing our results with the AGARD Working Group #17 results.

AGARD Validation

The AGARD Working Group #17 used various axisymmetric and non-axisymmetric nozzle configuration surface pressure distribution test results to validate CFD codes. All of the CFD codes used in this study were validated using the AGARD results.

Figure 8 shows two of the AGARD nozzles used in this validation effort (ref. 9). The non-axisymmetric nozzle was referred to as B.4, and the axisymmetric nozzle was referred to as B.1. Three validation cases were executed at Mach 0.94 including; (a) axisymmetric nozzle (B.1), attached flow, (b) axisymmetric nozzle (B.1), separated flow, and (c) non-axisymmetric nozzle

(B.4), separated flow. In general, the axisymmetric nozzle cases required significantly less computational resources than the non-axisymmetric case, and yielded consistent results for all of the CFD codes. While the axisymmetric cases were required for validation, the focus of this effort was placed upon the non-axisymmetric case, because this case closely resembled the non-axisymmetric DSM nozzle.

Figure 9 shows a comparison between nozzle B.4 centerline pressure coefficient test results and CFD predictions (ref. 9). Three plots are shown that graphically compare each of the three CFD codes involved in this study. The plots are set up to compare pressure coefficient as a function of non-dimensional distance (x/L) along the centerline, and the experimental results are identical for all three plots. From the NASTD plot, the conclusion can be drawn that NASTD accurately predicted the absolute values of experimental data as well as the trends with non-dimensional centerline distance. The NPARC plot using the Baldwin-Barth turbulence model also showed excellent agreement with the experimental data and closely resembled the NASTD prediction. In addition, the PAB3D plot exhibited excellent agreement with the experimental data. Note that PAB3D slightly overpredicted pressure coefficient near the trailing edge of the nozzle, and this could lead to a slight underprediction of drag coefficient for this specific case using a two equation, linear, k-ε turbulence model.

The results of Figure 9, coupled with the excellent agreement between CFD and experimental results for the axisymmetric cases (refs. 9, 10, 11 and 12), indicated that NASTD, NPARC and PAB3D were clearly capable of accurately predicting pressure coefficient distributions for HSCT type nozzles in the transonic flight regime. Thus, the CFD codes were validated with experimental pressure coefficient data. The next step was to ensure that the codes compared favorably with each other using the DSM nozzle.

HSCT DSM Nozzle Boattail Results

Prior to commencing the entire CFD study for all of the configurations shown in Figure 5, a baseline case was chosen to validate drag coefficient results between codes for an HSCT specific nozzle. The 16 degree boattail case with an 0.5 height ratio (1605) was chosen as the baseline case, primarily because this case effectively represented the median of the configuration matrix with respect to boattail flap angle. This case was studied by all four teams, and the results are presented below.

Figure 10 shows the Mach number contours along the centerline of the top flap of the 1605 nozzle at Mach 0.95. The flow was uniform prior to the nozzle hinge line. For this case, the external flow expanded around the nozzle boattail flap hinge line and recompressed through a normal shock wave just downstream of the expansion wave. Significant separation from the afterbody surface occurred behind the normal shock wave, and the flow did not reattach on the surface. Figure 11 shows the pressure contours and distribution as a function of non-dimensional flap length on the top nozzle flap surface for this configuration. Three different sections of the flap are presented on the pressure coefficient plot, with y/w=0.05 representing the flap centerline. Examining the centerline curve shows that the pressure coefficient reflected the effect of the expansion wave at approximately x/L=0.04, and the significant separation above x/L=0.16. Pressure coefficient distributions for all CFD codes exhibited the same trends for the 1605 nozzle at Mach 0.95, with slight variations in shock/expansion wave location.

Figure 12 shows the final drag coefficient results for the 1605 configuration at Mach 0.95. McDonnell Douglas results are represented by MDA-NAMP and MDA-ATAD. NASA Lewis and Langley results are represented by LeRC and LaRC, respectively. The Mach 0.95 case for all configurations was the most difficult Mach number regime to solve because of the high degree of separation. Consequently, the Mach 0.95 case for the 1605 configuration yielded the largest discrepancies between team member results of all the test cases. While there appeared to be significant disagreement between the results, most of the differences were due to technical factors and can be explained. First, note that the MDA-NAMP and LeRC results were within

10%. This was good agreement considering the highly unstable nature of this separated flow problem. The problem was complicated by the fact that the problem was subsonic, sonic and supersonic along a streamline, and the fact that the codes had to resolve exactly the location of the supersonic transition. Also, the agreement between MDA-NAMP and LeRC results was consistent with the AGARD validation results, which showed nearly identical pressure coefficient distributions for the non-axisymmetric nozzle at the Mach 0.94 condition. For this Mach 0.95 case, the boattail drag coefficient was approximated as the average of the MDA-NAMP and LeRC results.

The MDA-ATAD results for the 1605 configuration at Mach 0.95 should have been very close to the MDA-NAMP results due to the fact that NASTD was the flow solver for both cases. However, MDA-ATAD computations at Mach 0.95 yielded significantly lower pressure drag results than MDA-NAMP results. The MDA-ATAD solution of the 1605 configuration at Mach 0.95 encountered numerical convergence challenges that were attributable to the grid packing density in the vicinity of the nozzle boattail hinge line coupled with significant flow separation over the entire boattail surface. In addition, this was the first use of NASTD to solve transonic nozzle configurations with fully separated flow fields on a parallel network of distributed workstations. As a result, the MDA-ATAD engineers were operating as less experienced counterparts to the MDA-NAMP engineers concerning the operation of NASTD, and this contributed to the differences in results. (Reference 13 describes some of the impact on CFD results as a function of experience level.) These challenges persisted throughout the project for the MDA-ATAD Mach 0.95 solutions. The consensus of the team was that the MDA-ATAD solutions significantly underpredicted nozzle boattail drag at Mach 0.95, and should not be used.

The LaRC results for the 1605 configuration at Mach 0.95 were approximately 30% lower than the MDA-NAMP and LeRC results. This was consistent with the results from the AGARD validation study for the B.4 nozzle at Mach 0.94. It was noted above that PAB3D slightly overpredicted the B.4 nozzle pressure coefficient at the trailing edge of the nozzle, and that this could lead to an underprediction of nozzle boattail drag. In fact, this appeared to happen at Mach 0.95 for this configuration, and therefore the PAB3D value for the 1605 configuration at Mach 0.95 was approximately 30% low.

Figure 13 shows the Mach number contours along the centerline of the top flap of the 1605 nozzle at Mach 1.1. The flow was uniform prior to the nozzle hinge line. For this case, the external flow expanded around the nozzle boattail flap hinge line and recompressed through a normal shock wave located at approximately the halfway point of the nozzle flap length. Separation from the afterbody surface occurred behind the normal shock wave, and the flow did not reattach on the surface. The flow separation was not as severe as the Mach 0.95 case was, and the solution for the Mach 1.1 case was not as challenging as the previous Mach 0.95 solution. Figure 14 shows the pressure contours and distribution as a function of non-dimensional flap length on the top nozzle flap surface for this configuration. Examining the centerline (y/w=0.05) curve on the pressure coefficient plot shows that the pressure coefficient reflects the effect of the expansion wave at approximately x/L=0.04, and the separation above x/L=0.4. Note that the pressure recovery was not as significant for this configuration, compared to the Mach 0.95 case, which indicated that the Mach 1.1 case was a significantly less separated case that the Mach 0.95 case. Pressure coefficient distributions for all CFD codes exhibited the same trends for the 1605 nozzle at Mach 1.1, with slight variations in shock/expansion wave location.

Figure 15 shows the final drag coefficient results for the 1605 configuration at Mach 1.1. Because the separation for this case was less severe than the Mach 0.95 case, the CFD codes were better able to predict the flow characteristics, and the results were consistent. For example, the MDA-NAMP and NASA results agreed within 5%. Even more striking, the LeRC and LaRC results agreed within 0.5%. The MDA-ATAD results were approximately 10% lower than the MDA-NAMP results even though the grid was identical for both applications. The team chose to use the MDA-NAMP results due to the higher user experience level. For the Mach 1.1 case, the

boattail drag coefficient could accurately be predicted as the average of the MDA-NAMP, LeRC and LaRC results.

Figure 16 shows the Mach number contours along the centerline of the top flap of the 1605 nozzle at Mach 1.2. The flow was uniform prior to the nozzle hinge line. For this case, the external flow expanded around the nozzle boattail flap hinge line and recompressed through a normal shock wave located approximately three-quarters of the way down the nozzle flap length. Separation from the afterbody surface occurred behind the normal shock wave, and the flow did not reattach on the surface. The flow separation was less severe than the Mach 1.1 case, and therefore, the Mach 1.2 case was the most straightforward solution of the three Mach numbers studied. Figure 17 shows the pressure contours and distribution as a function of non-dimensional flap length on the top nozzle flap surface for this configuration. Examining the centerline (y/w=0.05) curve on the pressure coefficient plot shows that the pressure coefficient reflects the effect of the expansion wave at approximately x/L=0.04, and the separation above x/L=0.75. Note that the pressure recovery was not as significant for this configuration, compared even to the Mach 1.1 case, which indicated that the Mach 1.2 case had significantly less separation than the Mach 1.1 case. Pressure coefficient distributions for all CFD codes exhibited the same trends for the 1605 nozzle at Mach 1.2, with slight variations in shock/expansion wave location.

Figure 18 shows the final drag coefficient results for the 1605 configuration at Mach 1.2. Because the separation for this case was less severe than the other cases, the CFD codes were able to predict consistent results. For example, MDA-NAMP and NASA results agreed within 8%. Once again, the LeRC and LaRC results were essentially identical. Again, the MDA-ATAD results were approximately 8% lower than the MDA-NAMP results even though the grid was identical for both applications. The team chose to use the MDA-NAMP results due to the higher user experience level. For the Mach 1.2 case, the boattail drag coefficient could accurately be predicted as the average of the MDA-NAMP, LeRC and LaRC results.

Previously, the CFD codes were validated using experimental data. With the 1605 validation cases completed, the CFD codes were successfully validated with each other and proved that they could generate consistent results. However, future Mach 0.95 configuration solutions should be closely studied, and validation using similar geometries would be useful to understand the solutions. If the separation effects cause inconsistencies in the solutions, the solution should be used as an estimate not as the absolute answer. However, the Mach 1.1. and 1.2 solutions were clearly consistent. The other configurations could confidently be executed, and the absolute solutions could be used to help construct the IMS database.

Immediately after completion of the 1605 CFD code validation/comparison, each team developed solutions for the remaining configurations. The final results are shown in Figures 19 and 20. Figure 19 shows nozzle boattail drag coefficient as a function of Mach number for the 0.2 area ratio solutions. LaRC was responsible for the 2002 solutions (top line) while LeRC was responsible for the 1202 solutions (bottom line). The 2002 solution at Mach 0.95 was probably underpredicted based on the AGARD validation study results described earlier, and should be considered as an estimate for this specific case. The 1202 solution at Mach 1.2 was suspicious because nozzle boattail drag coefficient should be lower at Mach 1.2 than at Mach 1.1. This same anomaly was evident for both 12 degree boattail angle configurations. Figure 20 shows the solutions for the 0.5 area ratio solutions. MDA-NAMP was responsible for the 2005 solutions (top line), while MDA-ATAD was responsible for the 1205 solutions (bottom line). Again, the 1205 solutions appeared to be uniformly underpredicted by the amounts discussed in the validation study above, and should be used as estimates. The 1605 solutions (middle line) represented the average of the MDA-NAMP and LeRC solutions for Mach 0.95, and the average of the MDA-NAMP, LeRC and LaRC solutions for Mach 1.1 and 1.2. The solutions are tabulated in Table 1.

Comparison to IMS Database and Previous Method

As described earlier, the CFD results were to be used to substantiate and enhance the concurrent IMS database update activity. The following paragraphs describe the comparison between CFD, IMS database update and previous method results.

Before comparisons between CFD and IMS data are made, a brief comparison of IMS to experimental data will be discussed. Figure 3 showed a comparison between the previous boattail drag method and experimental data for a non-axisymmetric nozzle with a boattail flap angle of 16 degrees and an area ratio of 0.25. Figure 21 shows the same plot, but the new IMS database predictions have been added to the figure. The IMS database values showed excellent agreement with the non-axisymmetric experimental data for the entire range of radius of curvature ratio values. Figure 22 shows a comparison of IMS predictions for an axisymmetric nozzle with a 15 degree boattail flap angle and an area ratio of 0.45 (ref. 14). The IMS predictions agreed without bias with the experimental data for two different radius of curvature ratios (0.0 and 0.5). Finally, Figure 23 shows a comparison of IMS predictions for a non-axisymmetric nozzle with a radius of curvature ratio of 0.12 and an area ratio of 0.2 (ref. 15). Again, the IMS predictions agreed without bias with the experimental data for two different boattail flap angles (10 and 20 degrees). Based on these comparisons and additional supporting information (ref. 5), it was clear that the IMS prediction method with the recently updated database accurately predicted axisymmetric and non-axisymmetric nozzle boattail drag coefficient for complex geometry nozzles. Comparison with CFD results on HSCT specific nozzles shown below fully substantiated this new methodology for the HSCT project.

Figure 24 shows a comparison of the IMS, CFD and previous method predictions at Mach 0.95. Each of the six geometry configurations are shown individually on the bar graph. In general, the IMS and CFD predictions were comparable, and there was no apparent bias or trend with boattail angle or area ratio. Due to the fact that the Mach 0.95 case was highly separated and difficult to obtain CFD solutions for, the CFD results in Figure 23 should only be used to substantiate the IMS predictions. The previous method consistently underpredicted the IMS estimates by as much as 50%. No further conclusions can be drawn from this case.

Figure 25 shows the same comparison at Mach 1.1. In general, the IMS and CFD predictions agreed, but there was an apparent effect due to boattail angle. At a 12 degree boattail angle, the IMS prediction was slightly higher than the CFD prediction for the height ratio of 0.2. At a 16 degree boattail angle, the predictions also agreed very closely. At a 20 degree boattail angle, the CFD predictions were higher than the IMS predictions for both area ratios studied. It is likely that this trend was caused by sidewall effects, and is discussed below. The previous method consistently underpredicted the IMS estimates for boattail angles less than 20 degrees. For the 20 degree boattail angle cases, the previous method and the IMS predictions showed excellent agreement, but both represented estimates for nozzles without sidewalls.

The IMS and previous method predictions were based on non-axisymmetric nozzles without sidewalls. The CFD predictions used the DSM nozzle, which did have sidewalls. Based on the results of the CFD studies, the sidewalls on a non-axisymmetric nozzle may have caused a decrease in the pressure relief from the top of the nozzle flap to the ambient flow due to end-plating and vortex trapping effects, and thus may have caused an increase in drag coefficient. An example of this flow phenomena is shown in Figure 26, which depicts an aft facing forward view of the DSM nozzle. Higher pressure ambient flow is shown rising over the top of the sidewall and pressurizing the top of the nozzle boattail flap. If the sidewall were removed, the pressurizing of the flap may have increased, and the boattail drag coefficient may be reduced. One possible explanation of the trend shown in Figure 25 was that as boattail angle increased, the effect of the sidewall on the boattail flap increased. At 12 degrees, the sidewall did not appear to significantly impact the pressurization of the nozzle boattail flap. However, at 16 and 20 degrees boattail angle, the effect of the sidewall may have significantly impacted the prediction of nozzle boattail drag coefficient. A follow-on study is planned to update the IMS

database for sidewall effects. Also, a follow-on concurrent CFD study will evaluate the delta nozzle boattail drag coefficient due to removing the sidewalls using various configurations evaluated in this study.

Figure 27 shows the same comparison at Mach 1.2. In general, the IMS and CFD predictions agreed. Again, there was an apparent effect due to boattail angle, and the conclusion was consistent with the Mach 1.1 case. The sidewalls appeared to affect the 16 and 20 degree boattail angle CFD predictions. In addition, the previous method underpredicted IMS estimates for boattail angles less than 20 degrees, which was consistent with the Mach 1.1 results. Like the Mach 1.1 results, the previous method and IMS estimates agreed closely for the 20 degree boattail angle cases.

Figure 28 shows a comparison of CFD, IMS and previous method nozzle drag coefficient predictions normalized with total HSCT airplane drag coefficient for the 1202 configuration. All drag coefficients were referenced to the airplane wing area for this comparison, and the total airplane drag coefficient included the nozzle boattail drag element. For the 1202 configuration, the CFD and IMS predictions were of the same magnitude, and this substantiated that the previous method significantly underpredicted nozzle boattail drag coefficient. The previous method had predicted that nozzle boattail drag accounted for approximately 15% of the total airplane drag above Mach 1.0, while the CFD and IMS predictions showed that nozzle boattail drag accounted for 20-25% of the total airplane drag above Mach 1.0. Because the HSCT nozzle would likely operate at transonic boattail angles of approximately 12 degrees, the more accurate CFD and IMS predictions would significantly affect the aircraft transonic performance, and thus would impact the airplane sizing and mission performance.

Figure 29 shows the same comparison for the 1605 configuration. The CFD predictions were consistently larger than the IMS predictions for this case primarily because of the sidewall effects discussed earlier. However, the previous method underpredicted nozzle boattail drag for this configuration, and the replacement of the previous method with the IMS prediction methodology yielded a method that was more applicable to the HSCT nozzle trade studies because of the updated nozzle drag coefficient database and additional nozzle geometrical flexibility. On average, the IMS method predicted 15-20% higher boattail drag for this configuration than the previous method.

Figures 24-29 showed that the IMS and CFD predictions were in the same "ballpark" for the transonic Mach numbers tested, and thus, the IMS database was corroborated for use on the HSCT project. In addition, the previous method significantly underpredicted the nozzle boattail drag for boattail angles less than 20 degrees. The Mach 1.1 and 1.2 CFD predictions have been included in the transonic portion of the IMS database. Additional effort will be expended to update the IMS database for sidewall effects to better represent HSCT specific nozzles.

Lessons Learned

While the CFD study activity went smoothly and provided timely results, it was not without challenges and lessons learned. In fact, several challenges were overcome during the course of the study that can be avoided in future CFD activities.

The most significant lesson learned was that multiple CFD flow solvers could be used to compute results for a matrix of configurations. In this case, multiple flow solvers were used by multiple team members located throughout the country. The key to a successful program using this team approach involved setting up a stringent validation process. Prior to solving HSCT specific configurations, each flow solver was required to solve an established configuration (AGARD) with proven experimental data. Upon completion of this exercise, each team member was required to analyze the baseline configuration. The program did not begin in earnest until all team members agreed on the results from analyzing the baseline configuration. This strategy worked well for this team, and proved that multiple CFD flow solvers can be used. The major

benefit of this strategy was that it distributed the computational resource requirements throughout the team, and reduced the overall time required for the entire program.

In order to minimize differences in the results between flow solvers, the inputs must be kept as standardized as possible. In general, that meant using the same grids and the same type of turbulence model. The CFD grids should all be generated by the same organization, and should be thoroughly checked out using one of the flow solvers prior to distribution to the rest of the team. Small changes could be made to the grids by each team member to better suit their respective flow solver, but these changes should be kept to a minimum to reduce the possibility of grid dependent differences in the solutions. Also, similar turbulence models should be used to ensure that result differences do not stem from the difference in turbulence models. This effect could be significant for highly separated configurations.

Configurations with freestream Mach numbers close to 1.0, and large boattail angles posed serious challenges and limitations. Current CFD codes and turbulence models had difficulty solving equations when the flow was highly separated, and this affected shock position and pressure recovery. Thus, solutions to these types of configurations tended to be grid dependent.

In general, converged solutions to the above configurations required approximately 1 month of calendar time per case for the final results. The clock started when the initial grid was received and stopped when the final converged solution was achieved.

Perhaps the most important elements for success were the intangible elements. This effort was coordinated and managed effectively. Bi-weekly telecons and a goal-oriented schedule resulted in a focused program, and provided timely results that could be used to directly upgrade an element of HSCT propulsion system performance prediction methodology.

SUMMARY

Nozzle boattail drag is significant for the High Speed Civil Transport (HSCT) and can be as high as 25% of the overall propulsion system thrust at transonic conditions. Thus, nozzle boattail drag has the potential to create a thrust-drag pinch and can reduce HSCT aircraft aerodynamic efficiencies at transonic operating conditions. In order to accurately predict HSCT performance, it is imperative that nozzle boattail drag be accurately predicted.

A team of engineers used various CFD codes and provided consistent, accurate boattail drag coefficient predictions for a family of HSCT nozzle configurations. Three CFD flow solvers were used, and were validated using Advisory Group for Aerospace Research and Development (AGARD) data, and a baseline HSCT nozzle configuration. Each configuration studied incorporated a 3765 mixed flow turbofan and an axisymmetric inlet. Twenty seven total CFD cases were run, and each case was comprised of approximately 1.5 million data points. Pressure drag on the boattail surfaces was computed, and nozzle boattail drag coefficient was generated via a post-processed pressure integration. All CFD cases were successfully completed in a timely fashion.

The CFD solutions were grid dependent for the Mach 0.95, large boattail angle cases. These cases experienced significant separation, and resulted in a large variation in team results for the baseline configuration. The CFD results at Mach 1.1 and 1.2 were well defined, and there was excellent agreement between team results. NASA LeRC and LaRC results showed excellent agreement for these cases. The CFD and Integral Mean Slope (IMS) method results at Mach 0.95 generally agreed within 30%, but no clear bias was apparent in the comparison. Therefore, the Mach 0.95 CFD results were only used to substantiate the approximate magnitude of the IMS predictions at Mach 0.95. The Mach 1.1 and 1.2 CFD results were generally within 20% of the IMS predictions, but showed a bias that could have been caused by the DSM nozzle

sidewalls. The CFD predictions included nozzle sidewalls, while the IMS database did not include sidewalls. Because of this difference, the CFD predicted slightly higher nozzle drag coefficients for higher boattail angle cases (16 and 20 degrees), and this was consistent with the expected sidewall flow effect. Future work with CFD will quantify the sidewall effect, and incorporate this effect into the IMS database. For the Mach 1.1 and 1.2 cases, the CFD results substantiated the magnitude of the IMS predictions, and were incorporated as part of the nozzle drag coefficient database for use in future HSCT propulsion system performance calculations.

For this study, the CFD flow solvers accurately predicted isolated nozzle boattail pressure profiles and boattail drag coefficients. Consistent results were obtained using the three different flow solvers. The results corroborated with the IMS database and provided a more applicable method for accurate prediction of transonic HSCT nozzle boattail drag.

ACKNOWLEDGMENTS

The authors wish to thank the following team members for their dedicated effort. The success of this study is directly related to the excellent quality of the results generated by the following personnel; Nick Georgiadis, Fred Smith and Joe Holcomb of NASA Lewis Research Center; Khaled Abdol-Hamid, John Carlson, and Peter Coen of NASA Langley Research Center; Ray Cosner, Chris Culbertson, Greg Finfrock, Jay Jones, Rob Jonietz, Walt LaBozzetta, Bill Regnier and Hoyt Wallace of McDonnell Douglas Aerospace.

REFERENCES

1. Silhan, F.V., and Cubbage, J.M., "Drag of Conical and Circular-Arc Boattail Afterbodies at Mach Numbers from 0.6 to 1.3", NACA Research Memorandum RM L56K22, January 1957.

2. Bangert, L.S., and Carson, G.T. Jr., "Effect of Afterbody Geometry on Aerodynamic Characteristics of Isolated Nonaxisymmetric Afterbodies at Transonic Mach Numbers", NASA Technical Paper TP 3236, September 1992.

3. Stevens, H.L., Thayer, E.B., and Fullerton, J.F., "Development of the Multi-Function 2-D/C-D Nozzle", AIAA Paper 81-1491, July 1981.

4. Wallace, H.W., Hiley, P.E., Reinsberg, J.G., and Booher, M.E., "Advanced Nozzle Concepts Program Final Report; Summary of Results and Nozzle Integration Design Criteria", AFWAL-TR-81-3165, Volume I, January 1982.

5. Wallace, H.W., "Nozzle Boattail Drag Topics", Presentation (unpublished) to the Propulsion System Evaluation Team of the NASA Lewis Research Center Critical Propulsion System Components Program, St. Louis, MO, March 1995.

6. Cooper, K., "NPARC 2.0 Features and Capabilities", AIAA 95-2609, Presented at the 31st Joint Propulsion Conference, July 10-12, 1995.

7. Abdol-Hamid, K.S., Carlson, J.R., and Lakshmanan, B., "Application of Navier-Stokes Code PAB3D to Attached and Separated Flows with a k-ε Turbulence Model", NASA Technical Paper TP 3840, 1994.

8. Bush, R. H., "A Three-Dimensional, Zonal, Navier-Stokes Code for Subsonic Through Hypersonic Propulsion Flow Fields", AIAA 88-2830, Presented at the 24th Joint Propulsion Conference, July 1988.

9. AGARD Fluid Dynamics Panel (Working Group #17): Aerodynamics of 3D Aircraft Afterbodies, AGARD Advisory Report AR-318, September, 1995.

10. Carlson, J.R., Pao, S.P., Abdol-Hamid, K.S., and Jones, W.T., "Aerodynamic Performance Predictions of Single and Twin-Jet Afterbodies", AIAA 95-2622, Presented at 31st Joint Propulsion Conference, July 1995.

11. Compton, W.B. III, Abdol-Hamid, K.S., and Abeyounis, W.K., "Comparison of Algebraic Turbulence Models for Afterbody Flow with Jet Exhaust", AIAA Journal, Volume 30, pp. 2716-2722, November 1992.

12. DeBonis, James R., Georgiadis, Nicholas J., Smith, Crawford F., "Validation of the NPARC Code for Nozzle Afterbody Flows at Transonic Speeds", NASA Technical Memorandum 106971, Presented at the 31st Joint Propulsion Conference, July 10-12, 1995.

13. Cosner, R.R., "CFD Validation Requirements for Technology Transition", AIAA 95-2227, Presented at 26th AIAA Fluid Dynamics Conference, June 19-22, 1995.

14. Shrewsbury, G.D., "Effect of Boattail Juncture Shape on Pressure Drag Coefficients of Isolated Afterbodies", NASA TM X-1517, March 1968.

15. Carlson, J.R., and Asbury, S.C., "Two-Dimensional Converging-Diverging Rippled Nozzles at Transonic Speeds", NASA Technical Paper TP 3440, July 1994.

Config	Boattail Angle (β) (deg)	h_9/h_{10}	Mach No.	Cd boattail	Boattail Drag (lbs)	Team Member	CFD Code
N1202	12	0.2	0.95	0.1087	550.0	LeRC	NPARC
N1202	12	0.2	1.1	0.1827	1238.8	LeRC	NPARC
N1202	12	0.2	1.2	0.1840	1484.7	LeRC	NPARC
N1205	12	0.5	0.95	0.0501	253.5	MDA-ATAD	NASTD
N1205	12	0.5	1.1	0.0809	548.3	MDA-ATAD	NASTD
N1205	12	0.5	1.2	0.0985	794.7	MDA-ATAD	NASTD
N1605	16	0.5	0.95	0.0678	342.9	MDA-ATAD	NASTD
N1605	16	0.5	1.1	0.1847	1252.7	MDA-ATAD	NASTD
N1605	16	0.5	1.2	0.1645	1327.6	MDA-ATAD	NASTD
N1605	16	0.5	0.95	0.1426	721.1	MDA-NAMP	NASTD
N1605	16	0.5	1.1	0.1969	1335.5	MDA-NAMP	NASTD
N1605	16	0.5	1.2	0.1802	1454.6	MDA-NAMP	NASTD
N1605	16	0.5	0.95	0.0939	474.9	LaRC	PAB3D
N1605	16	0.5	1.1	0.2094	1419.9	LaRC	PAB3D
N1605	16	0.5	1.2	0.1962	1583.6	LaRC	PAB3D
N1605	16	0.5	0.95	0.1284	649.4	LeRC	NPARC
N1605	16	0.5	1.1	0.2084	1413.5	LeRC	NPARC
N1605	16	0.5	1.2	0.1960	1581.8	LeRC	NPARC
N2002	20	0.2	0.95	0.1728	873.9	LaRC	PAB3D
N2002	20	0.2	1.1	0.3759	2548.9	LaRC	PAB3D
N2002	20	0.2	1.2	0.3594	2900.6	LaRC	PAB3D
N2005	20	0.5	0.95	0.1707	863.2	MDA-NAMP	NASTD
N2005	20	0.5	1.1	0.2414	1637.2	MDA-NAMP	NASTD
N2005	20	0.5	1.2	0.2209	1782.6	MDA-NAMP	NASTD

A_{10} = 6137 sq. in.

Table 1. - CFD Nozzle Boattail Drag Coefficient Solution Summary

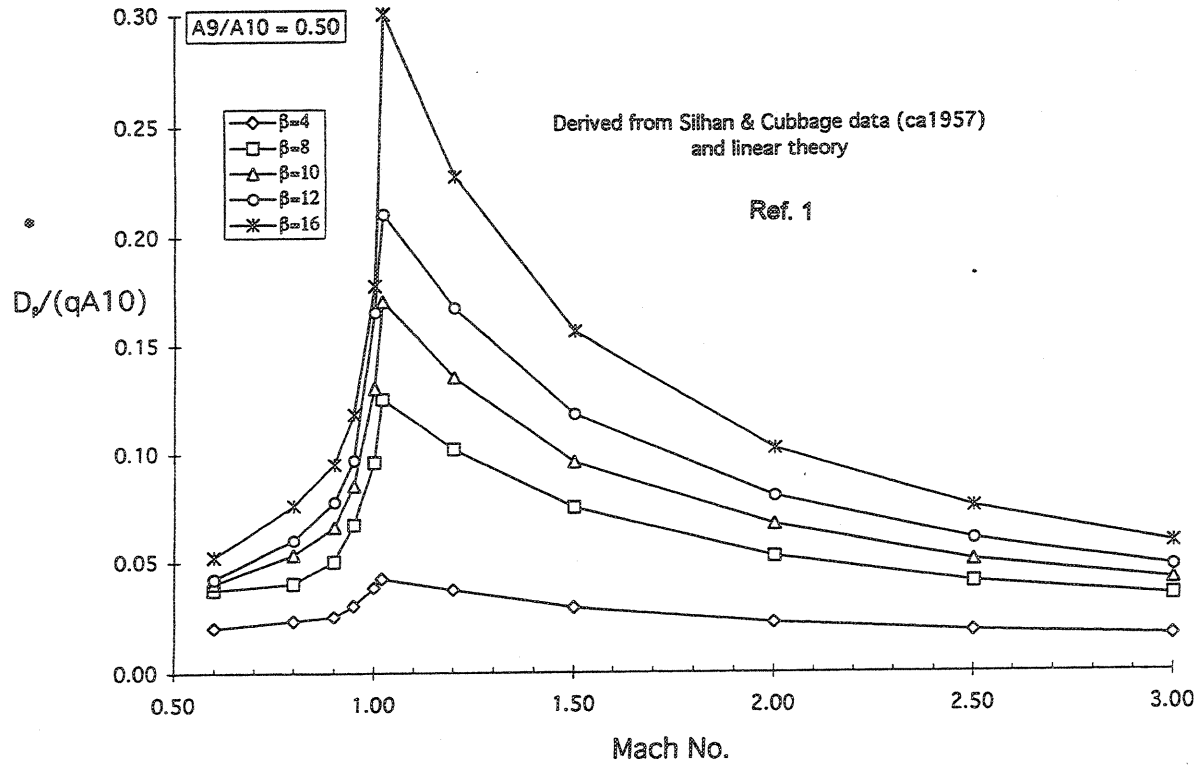

Figure 1. - LeRC/PW Nozzle Boattail Drag Coefficient Data for Rectangular Nozzles with A_ϕ/A_{10}=0.5.

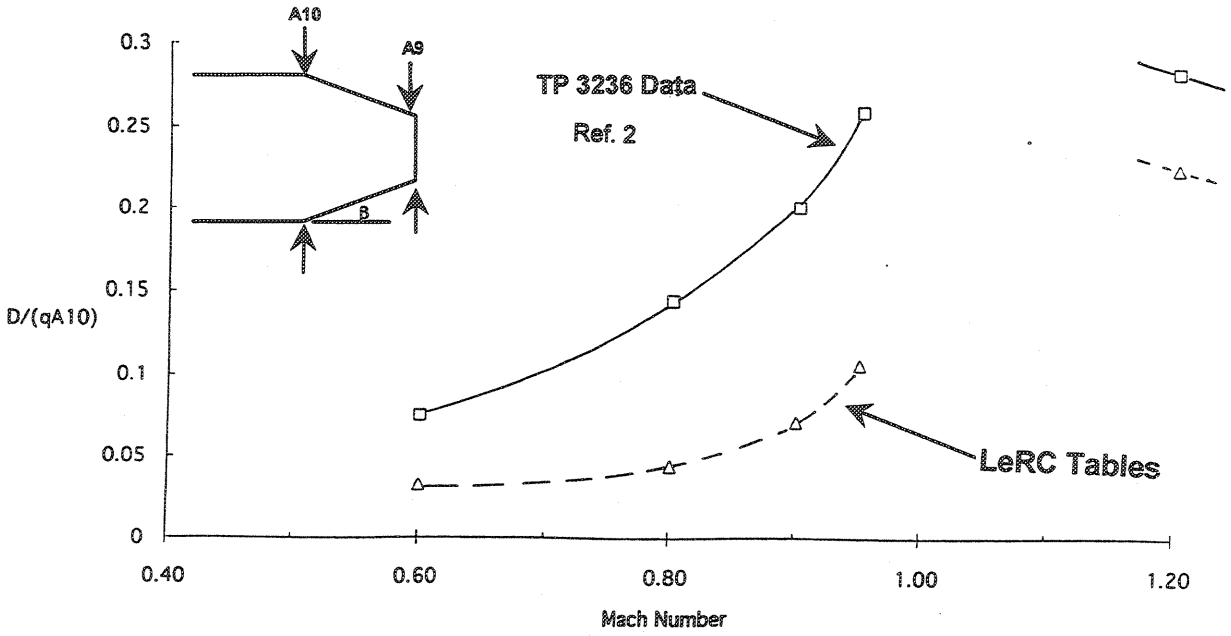

Figure 2. - Comparison of Previous Method Nozzle Boattail Drag Coefficient Predictions with 2D Nozzle Wind Tunnel Data as a Function of Mach Number (β=17.9 deg, A_ϕ/A_{10}=0.14).

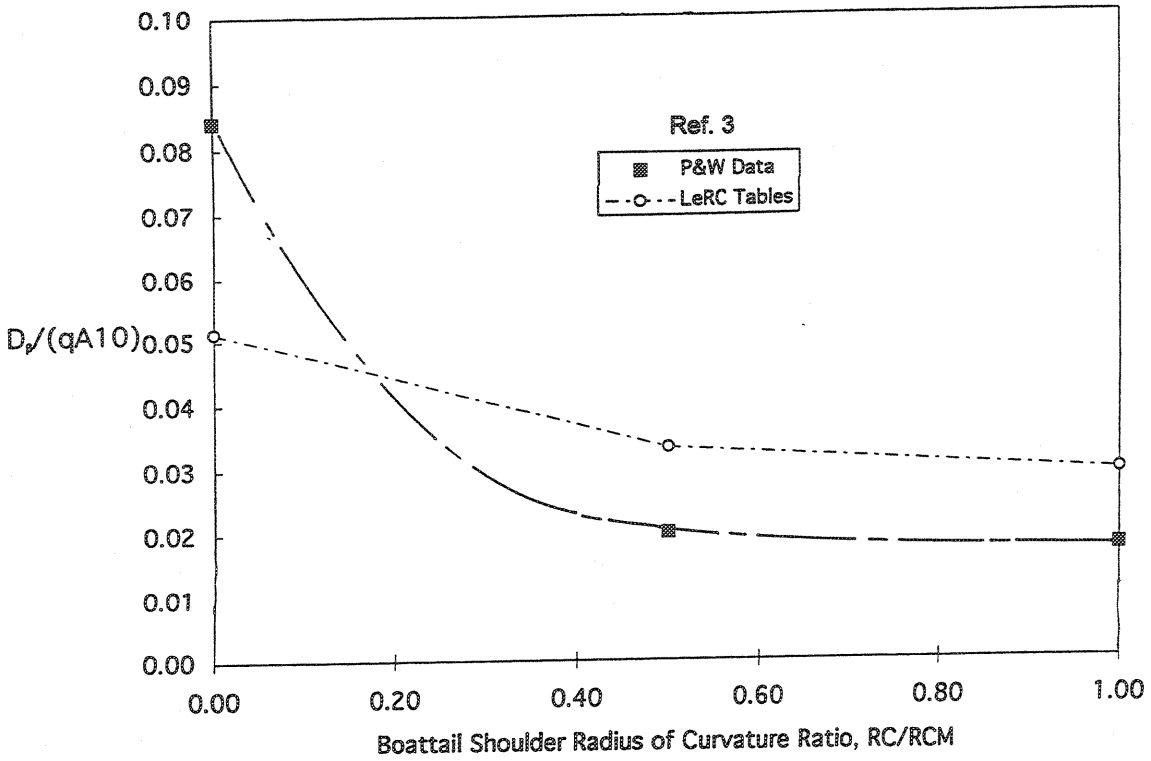

Figure 3. - Comparison of Previous Method Nozzle Boattail Drag Coefficient Predictions with 2D Nozzle Wind Tunnel Data as a Function of Radius of Curvature Ratio (β=16 deg, A_9/A_{10}=0.25, M=0.9).

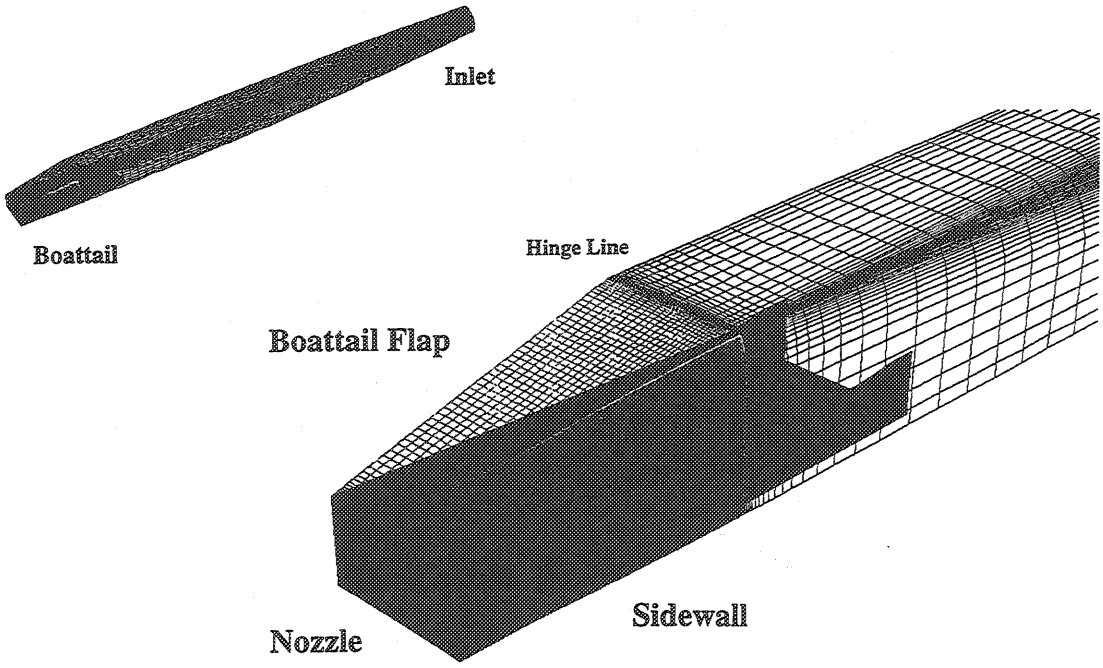

Figure 4. - Typical Isolated HSCT Nacelle Configuration Used in CFD Boattail Drag Study.

Configuration	h_9/h_{10}	Boattail	M_∞	Team
N0010	1.0	0°	0.95, 1.10, 1.20	NASA Langley
N1202	0.2	12°	0.95, 1.10, 1.20	NASA Lewis
N2002	0.2	20°	0.95, 1.10, 1.20	NASA Langley
N1205	0.5	12°	0.95, 1.10, 1.20	MDA–ATAD
N1605	0.5	16°	0.95, 1.10, 1.20	MDA–ATAD MDA–NAMP NASA Langley NASA Lewis
N2005	0.5	20°	0.95, 1.10, 1.20	MDA–NAMP

Figure 5. - Configuration Run Matrix.

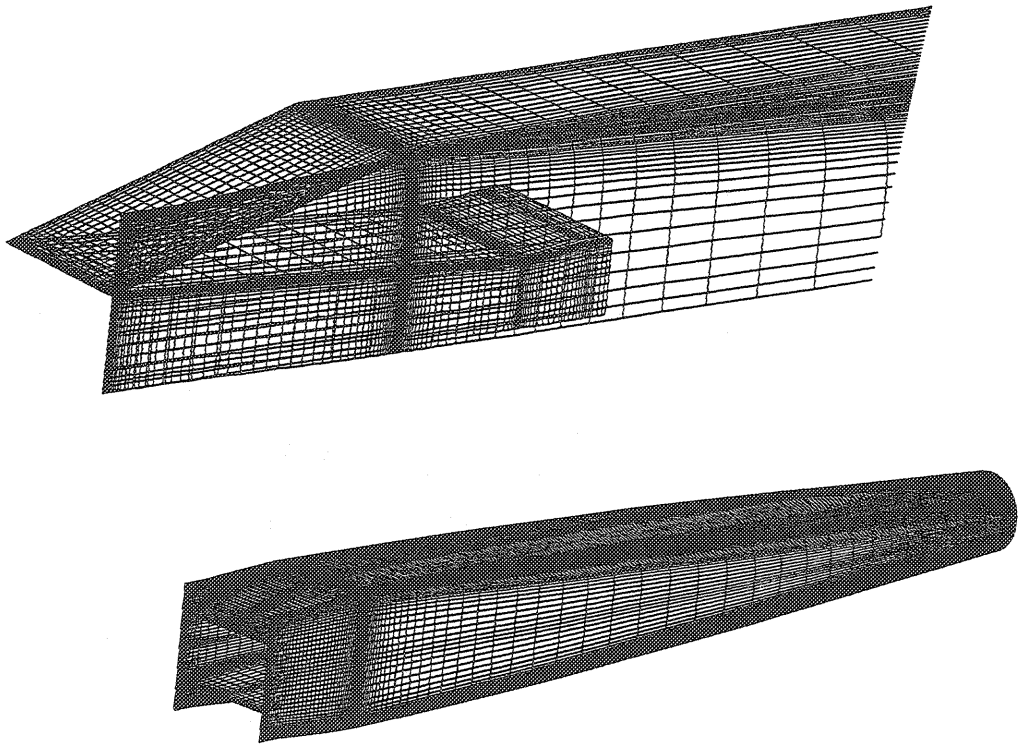

Figure 6. - Typical Full Scale Nacelle Surface Grid Definition.

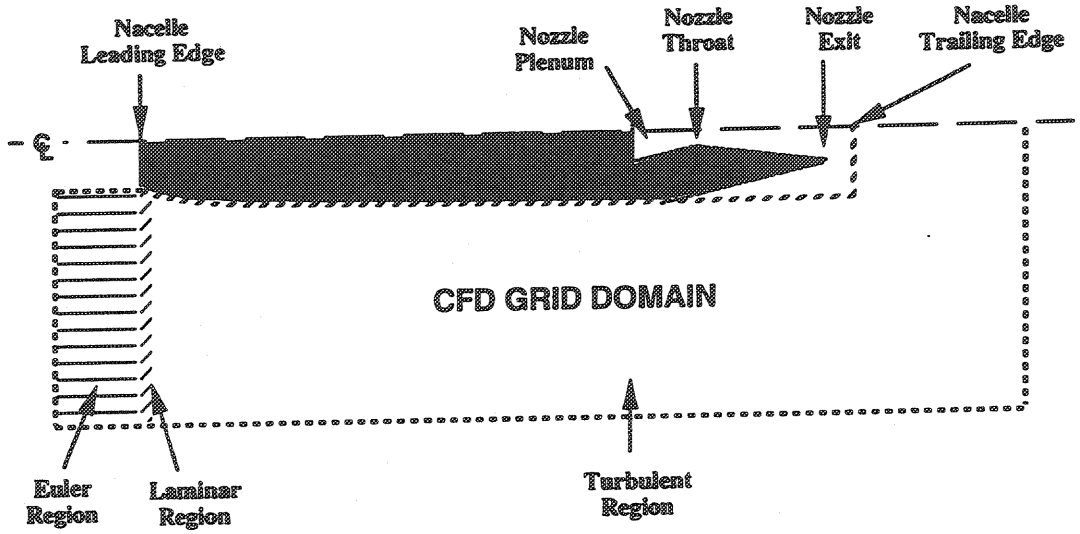

Figure 7. - CFD Flow Type Definition Groundrules.

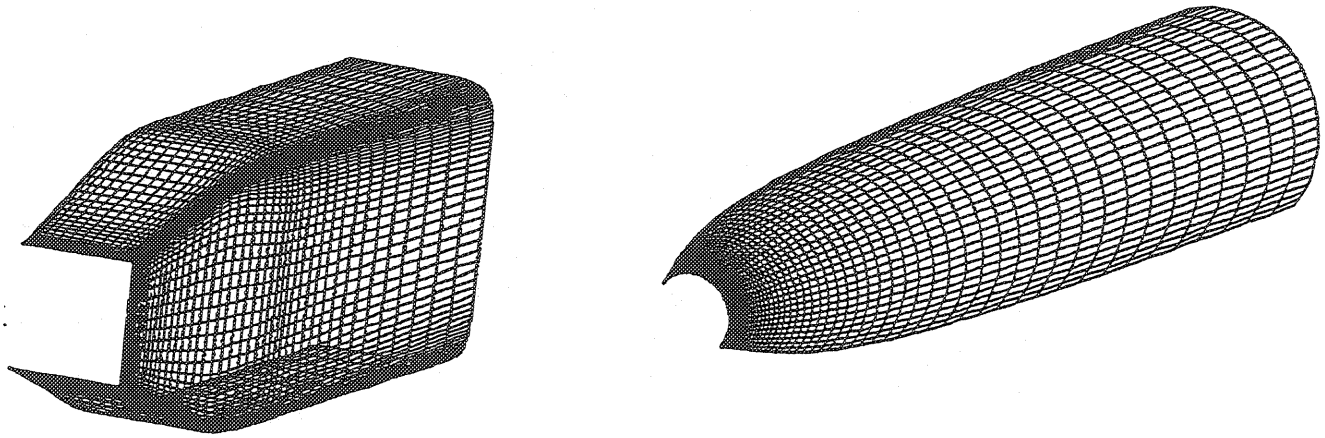

Ref. 9

2D B.4 Nozzle

Axisymmetric B.1 Nozzle

Figure 8. - AGARD Working Group #17 Test Case Nozzle Grid Definitions.

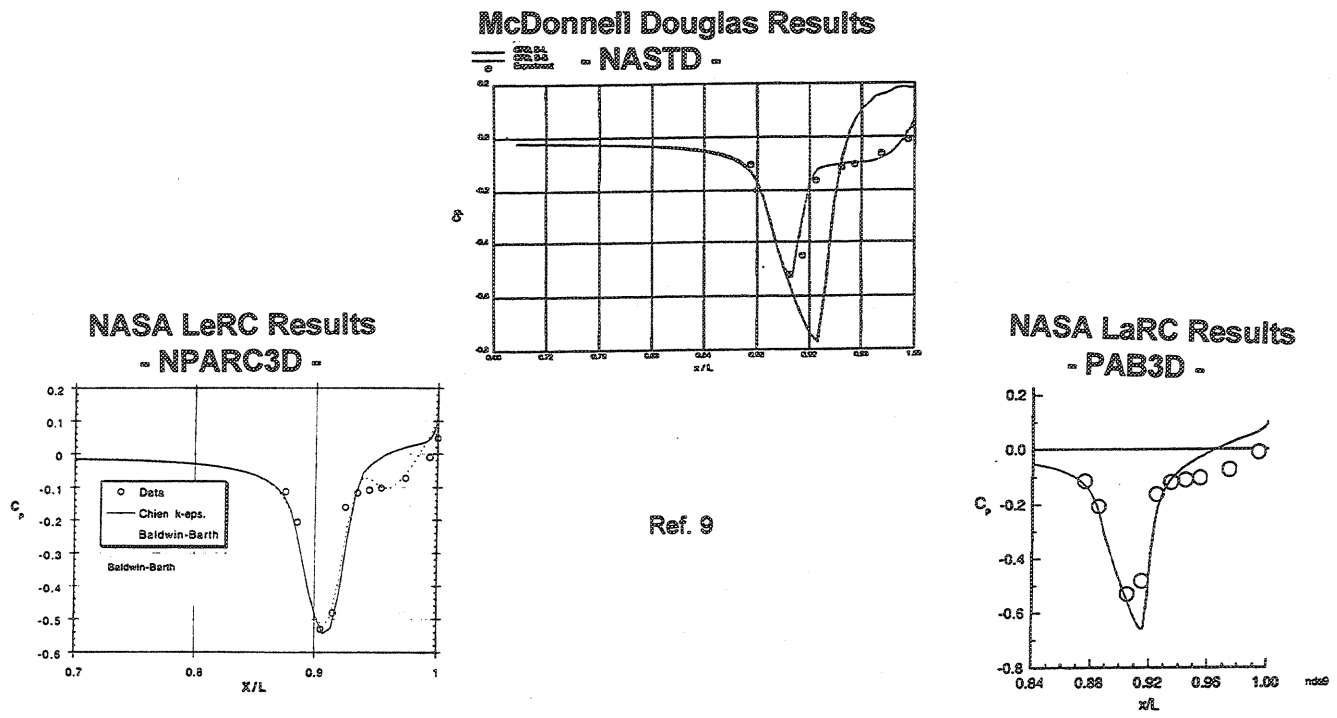

Figure 9. - Comparison of CFD Flow Solver Results with AGARD Working Group #17 B.4.2 2D Nozzle Test Data.

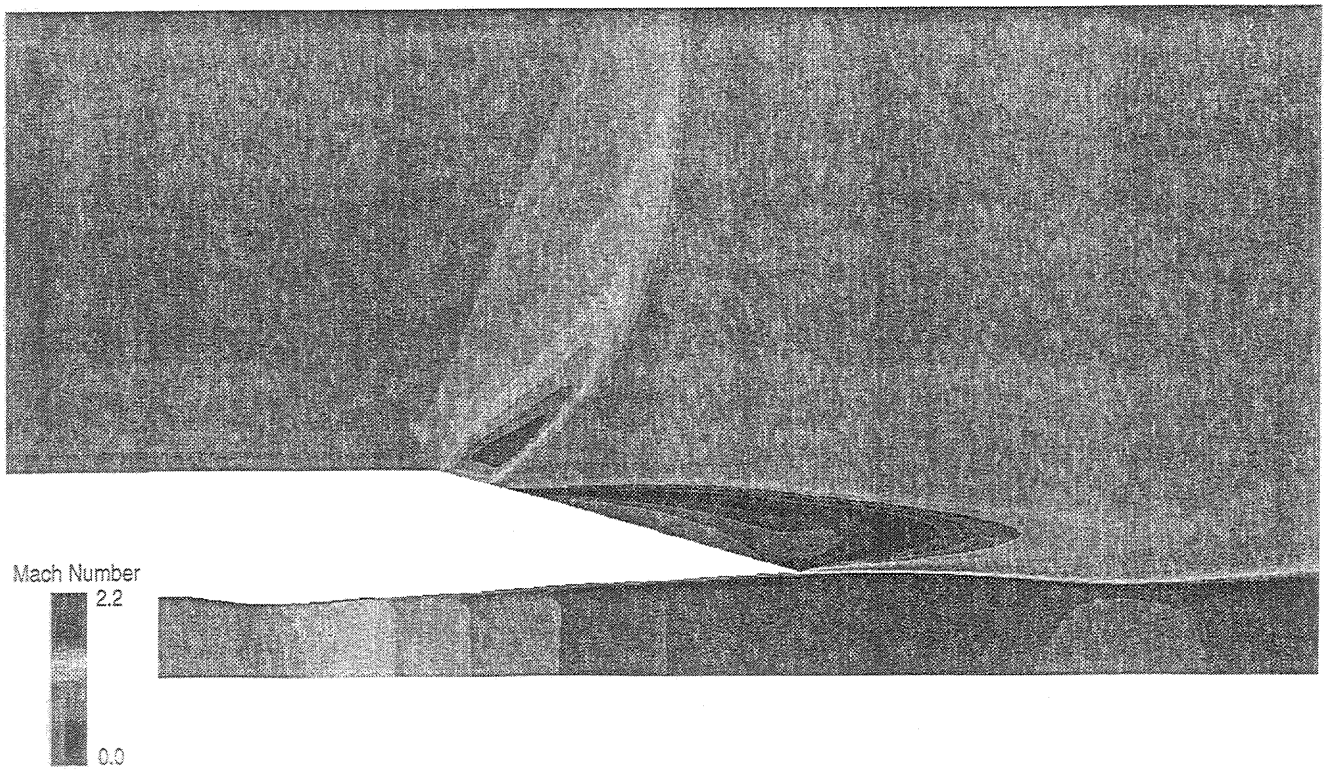

Figure 10. - Mach Number Contours Along Centerline for 1605 Configuration at M=0.95.

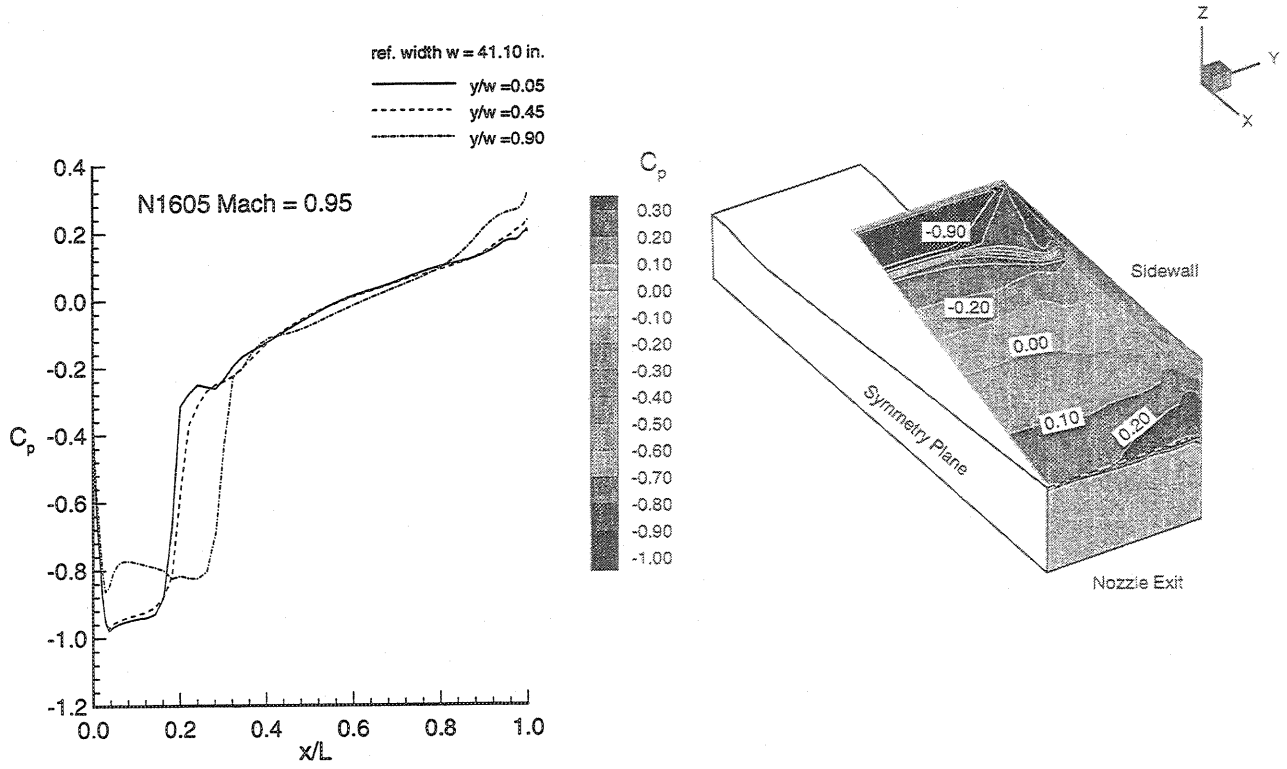

Figure 11. - Pressure Contours and Distributions for 1605 Configuration at M=0.95.

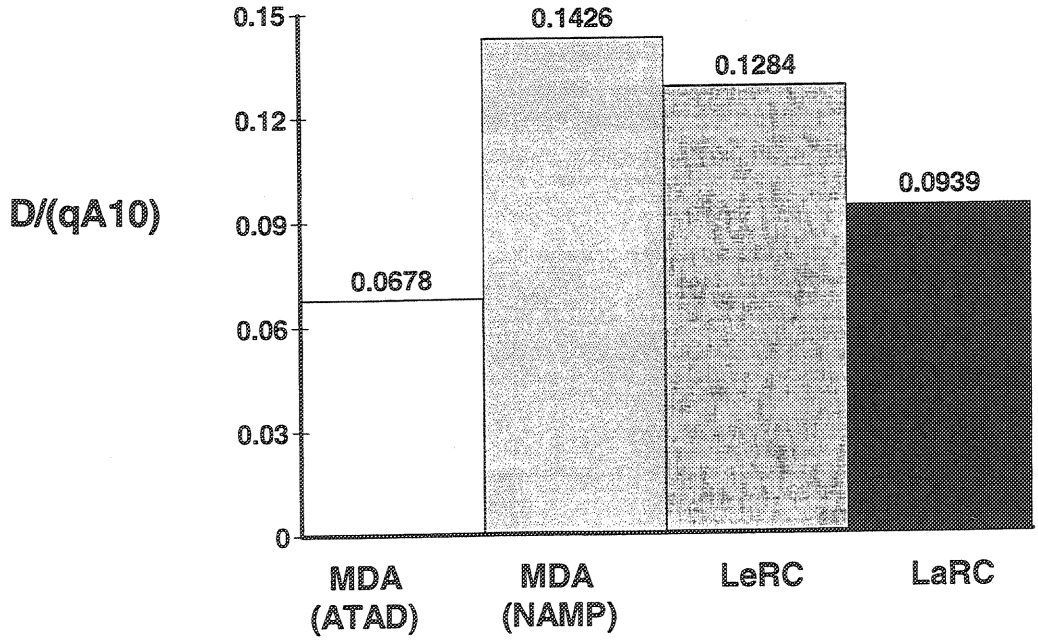

Figure 12. - Final CFD Nozzle Drag Coefficient Results for 1605 Configuration at M=0.95.

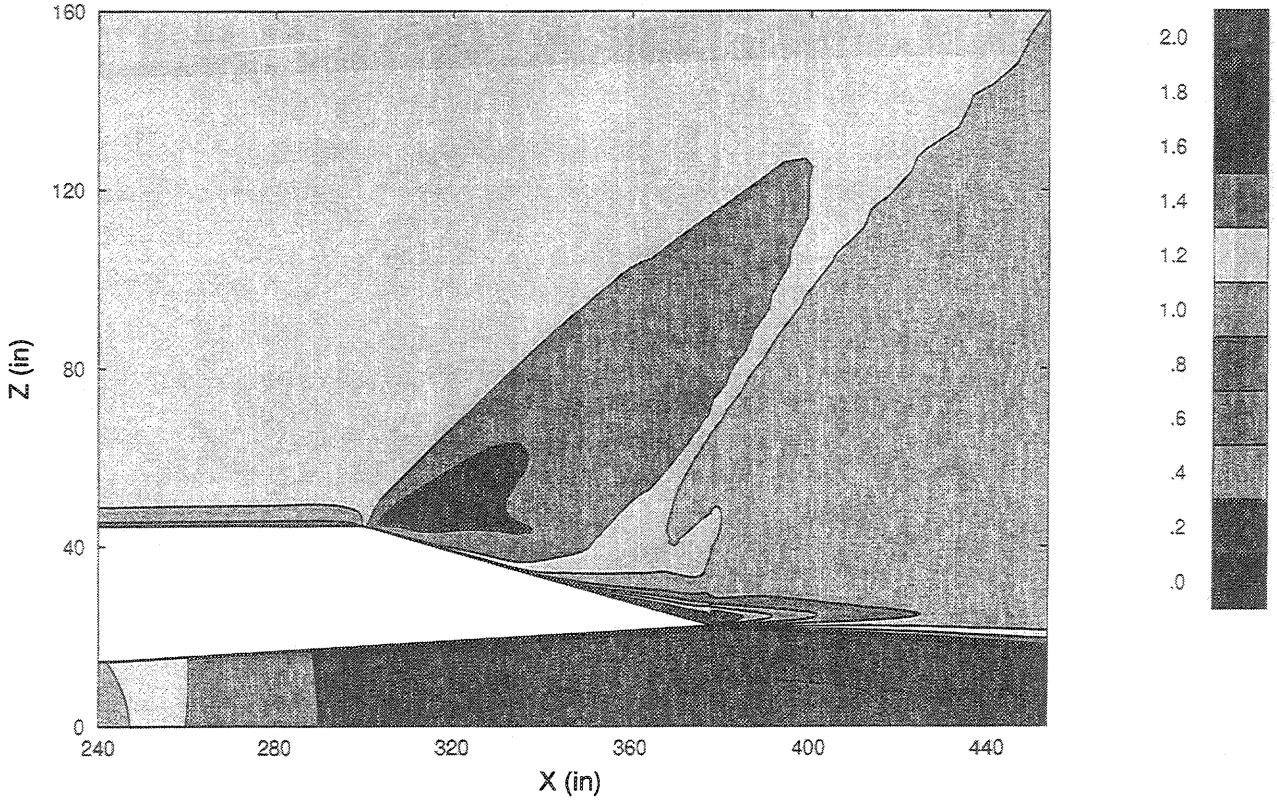

Figure 13. - Mach Number Contours Along Centerline for 1605 Configuration at M=1.1.

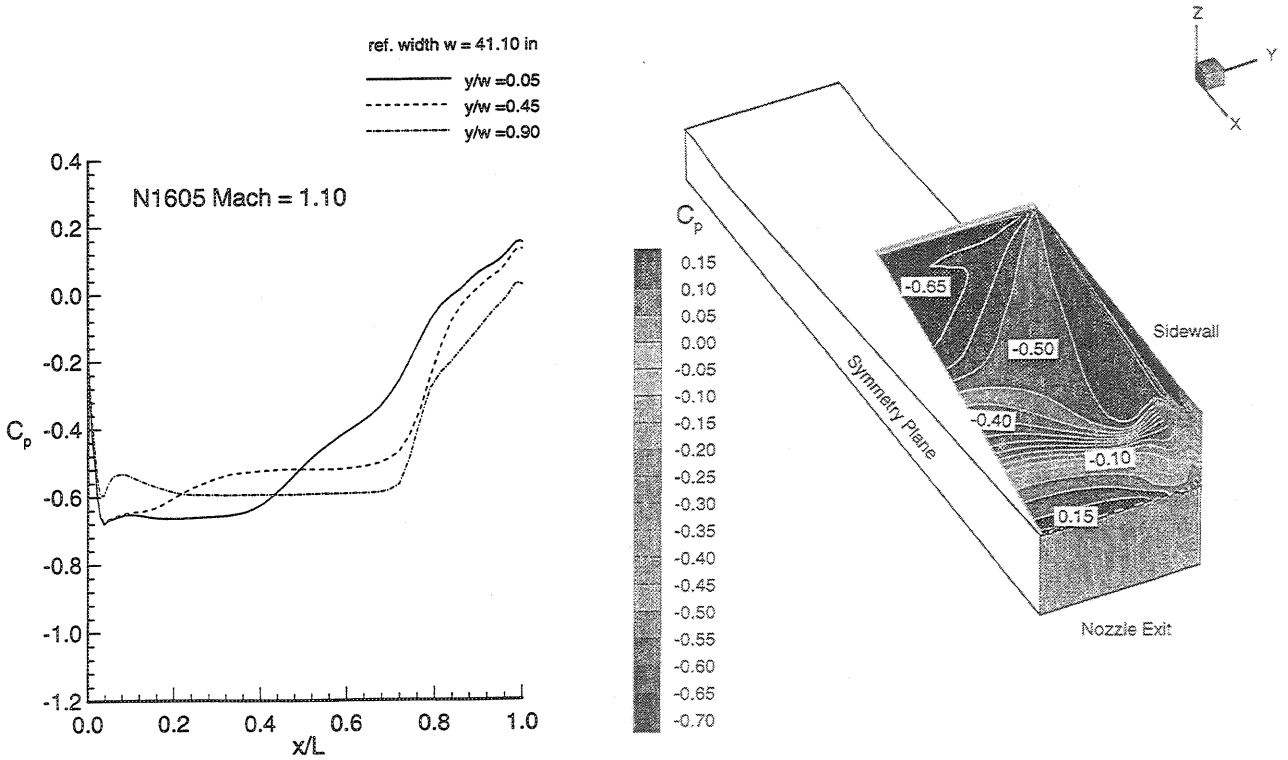

Figure 14. - Pressure Contours and Distributions for 1605 Configuration at M=1.1.

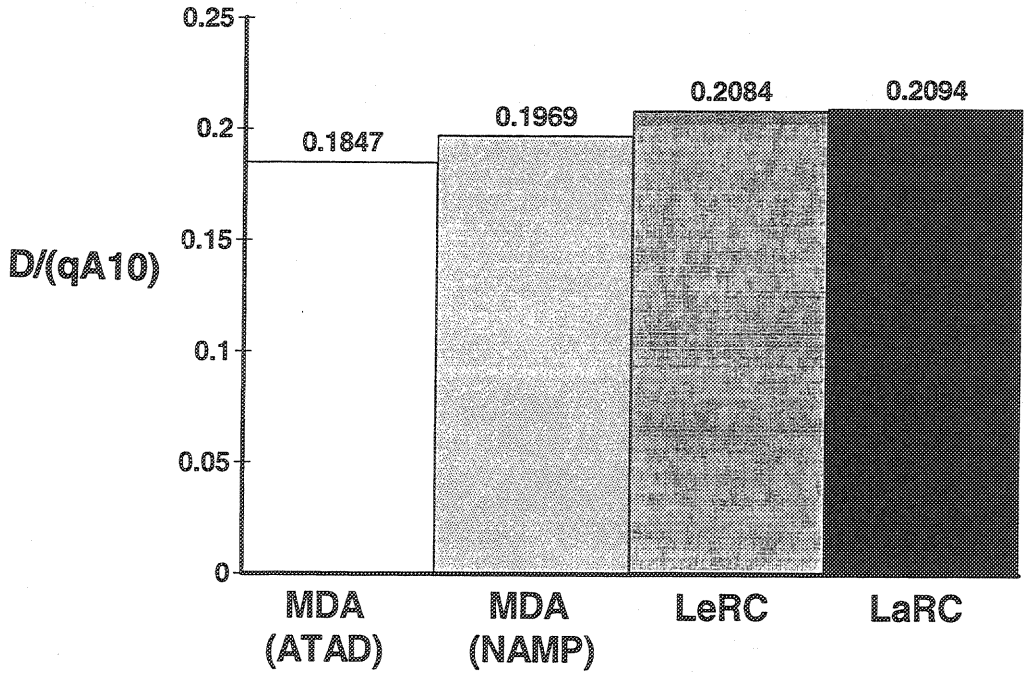

Figure 15. - Final CFD Nozzle Drag Coefficient Results for 1605 Configuration at M=1.1.

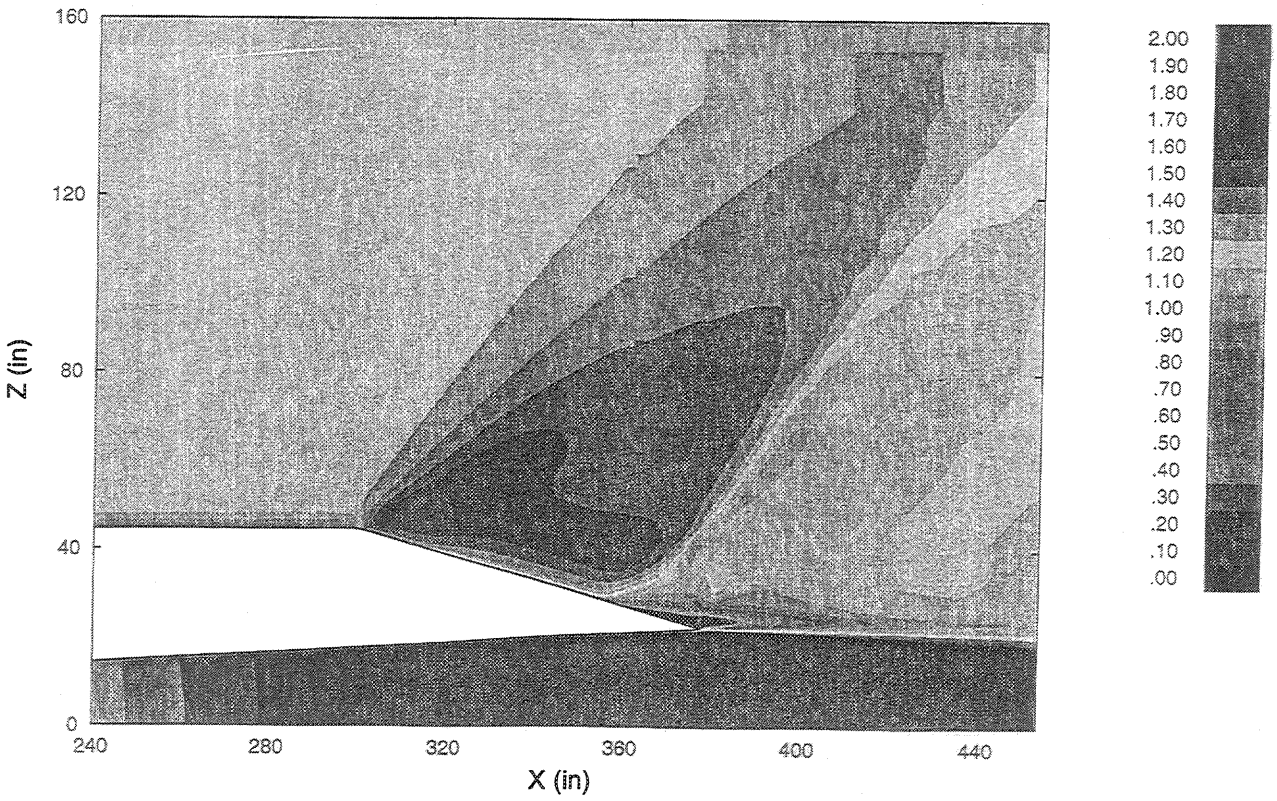

Figure 16. - Mach Number Contours Along Centerline for 1605 Configuration at M=1.2.

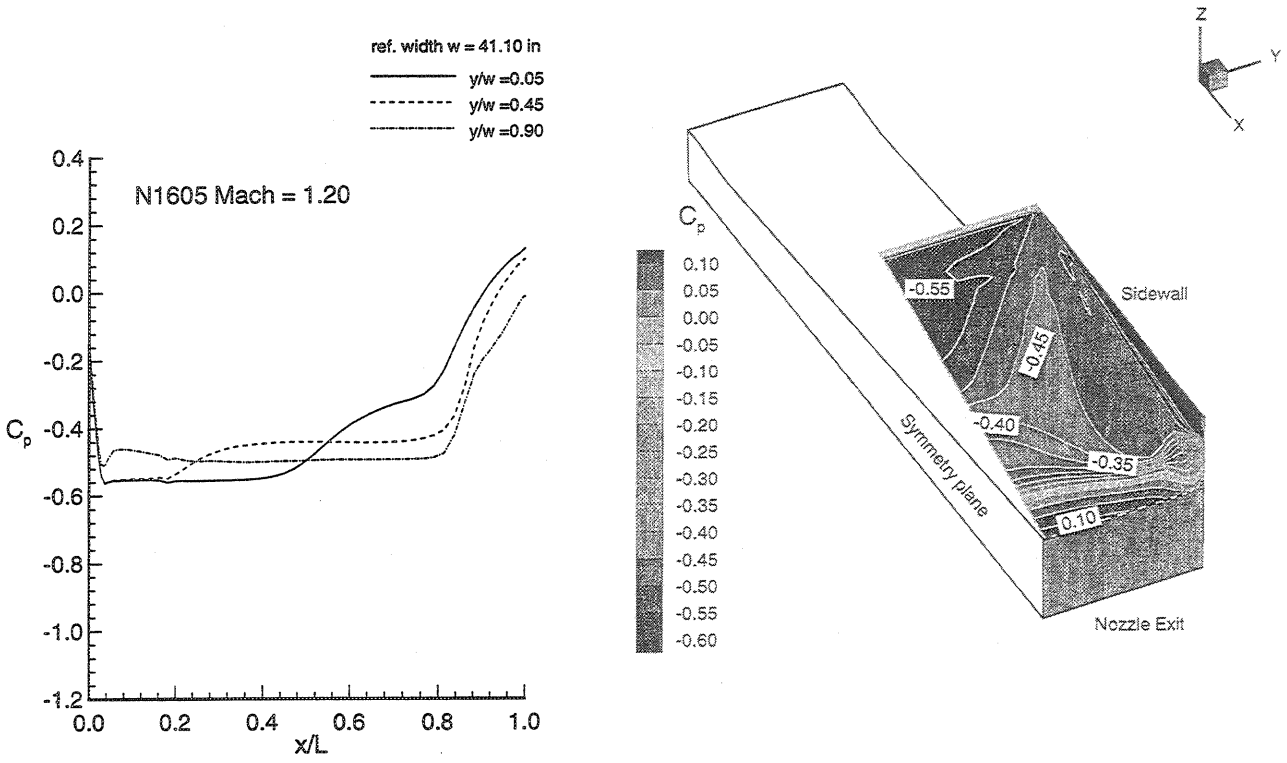

Figure 17. - Pressure Contours and Distributions for 1605 Configuration at M=1.2.

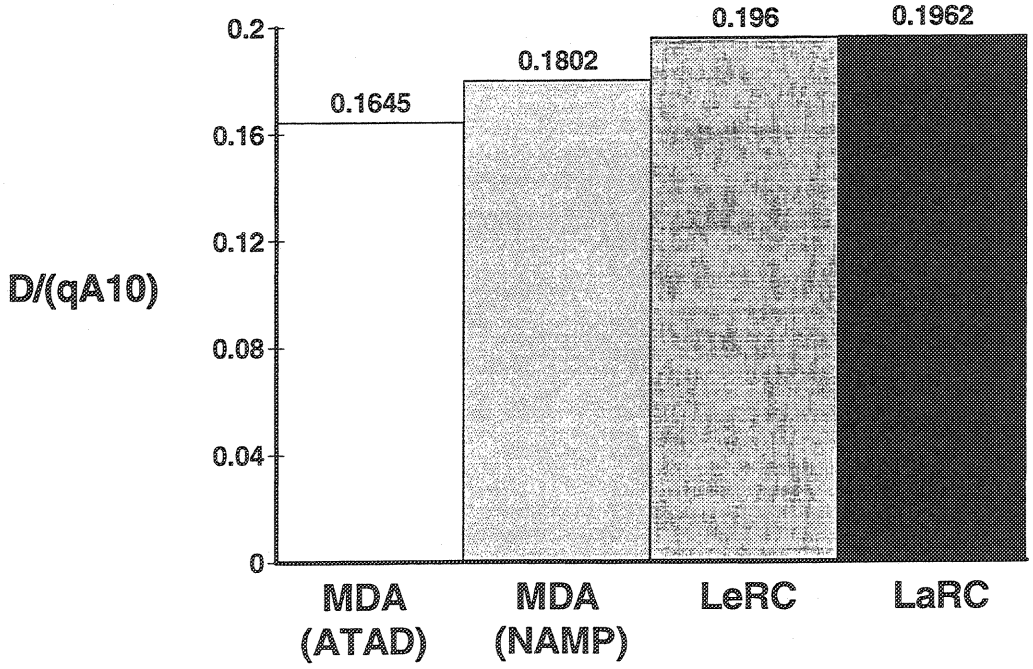

Figure 18. - Final CFD Nozzle Drag Coefficient Results for 1605 Configuration at M=1.2.

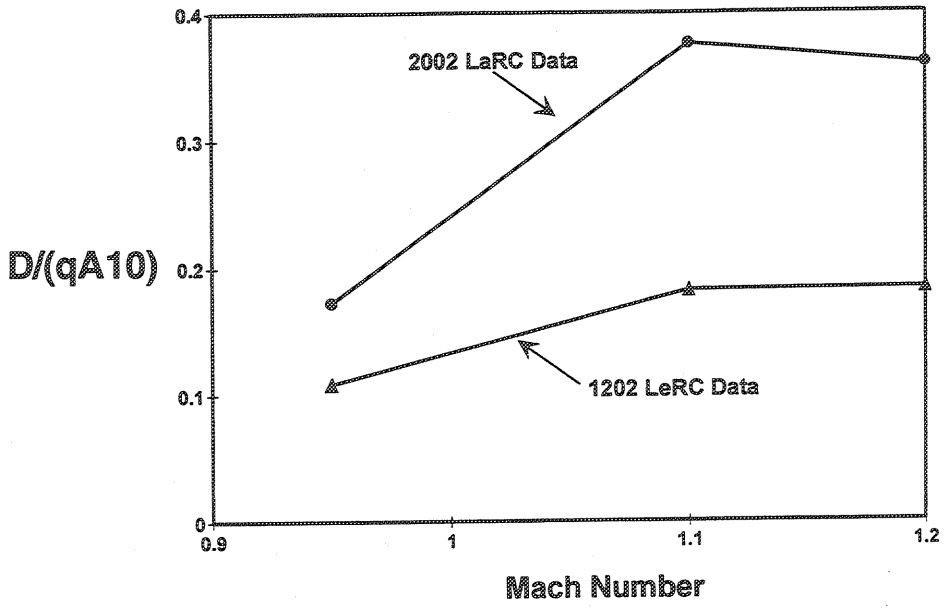

Figure 19. - Final CFD Nozzle Drag Coefficient Results for h_9/h_{10}=0.2 (A_9/A_{10}=0.187) Configurations.

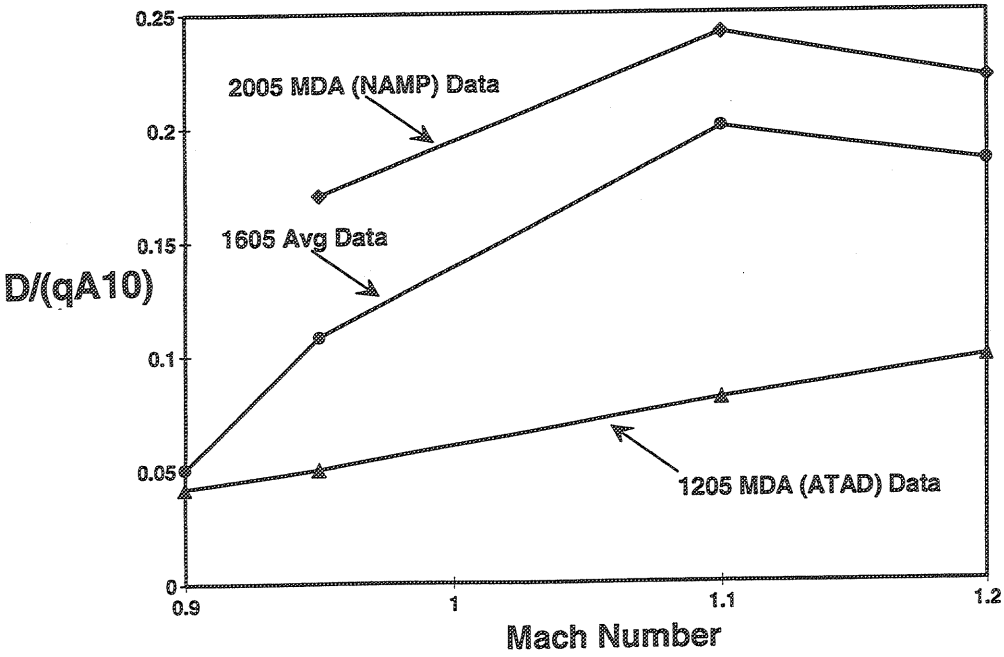

Figure 20. - Final CFD Nozzle Drag Coefficient Results for h_9/h_{10}=0.5 (A_9/A_{10}=0.467) Configurations.

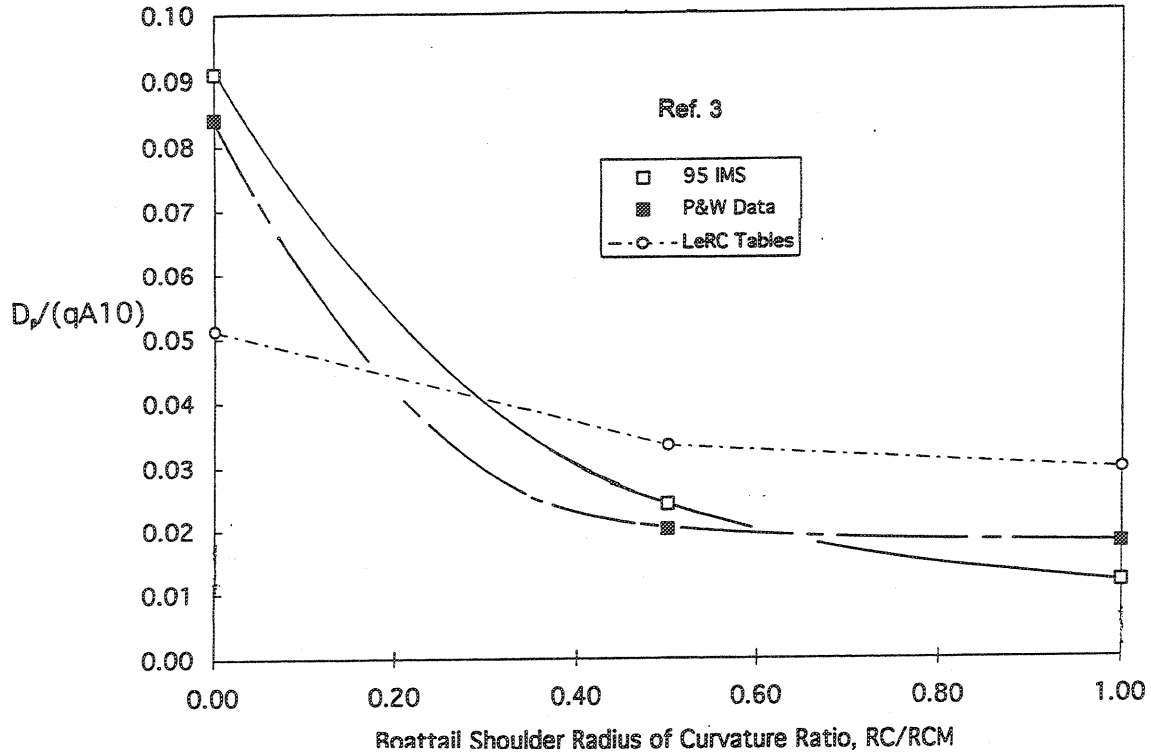

Figure 21. - Comparison of IMS Drag Predictions with 2D Nozzle Wind Tunnel Test Data as a Function of Radius of Curvature Ratio (β=16 deg, A_9/A_{10}=0.25, M=0.9).

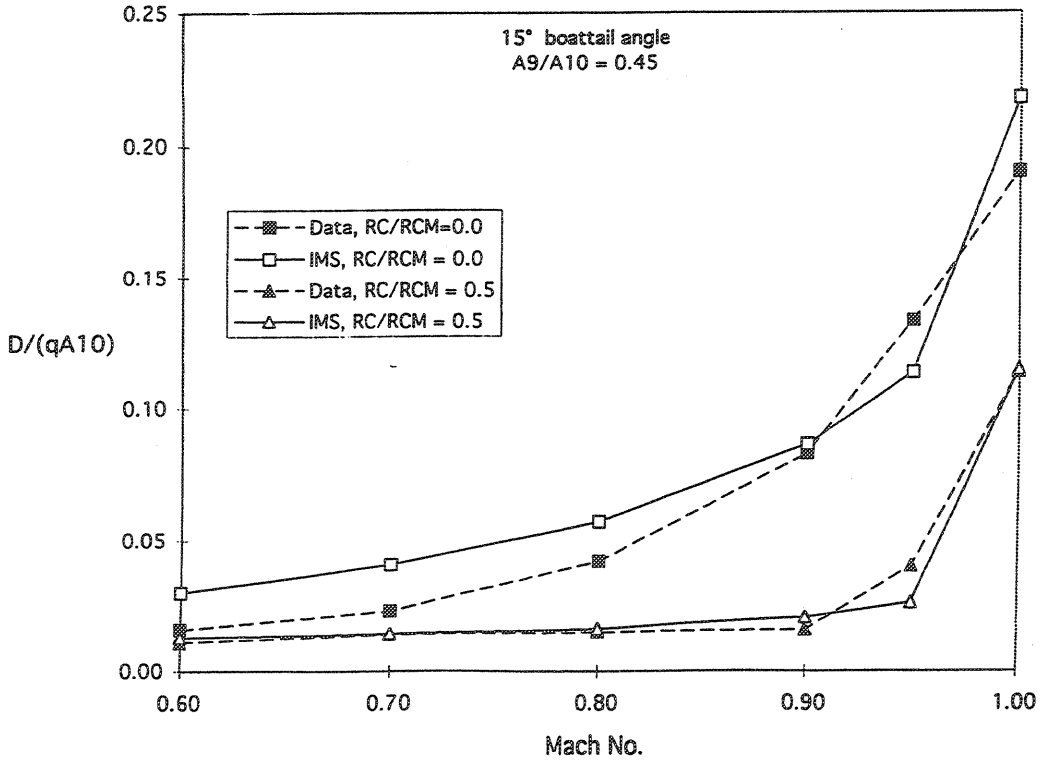

Figure 22. - Comparison of IMS Drag Predictions with Axisymmetric Nozzle Test Data (β=15 deg, A_9/A_{10}=0.45).

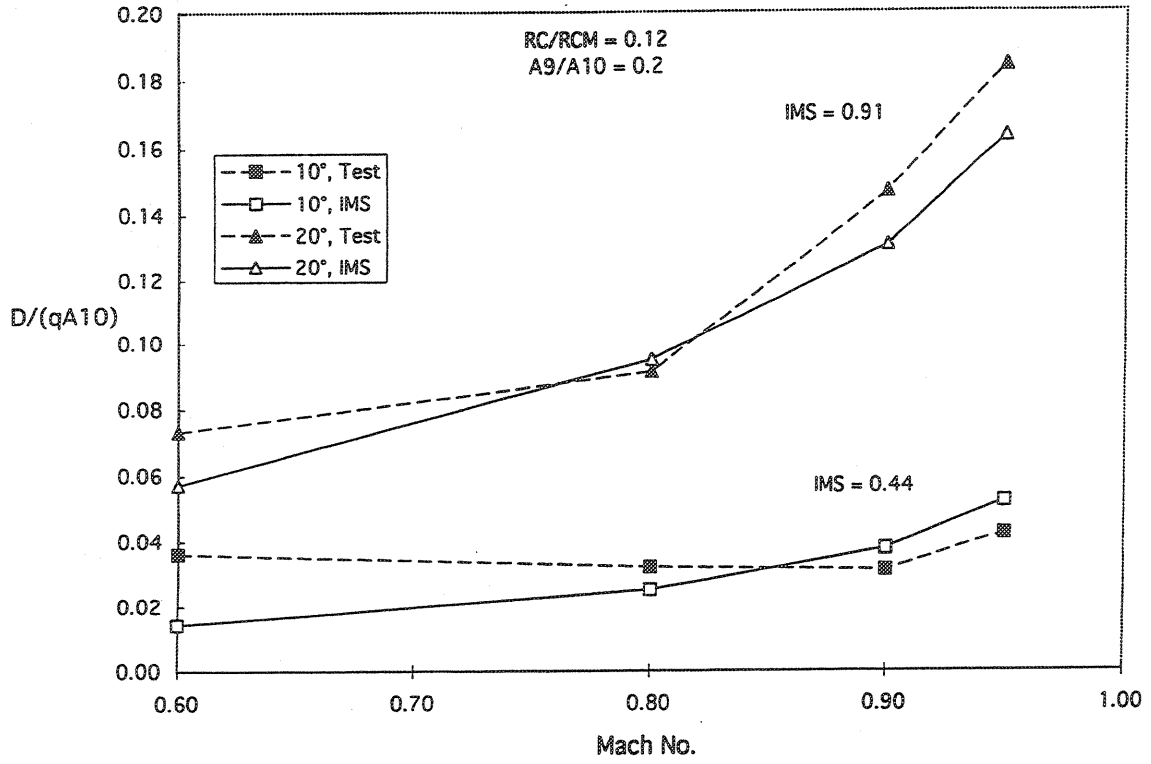

Figure 23. - Comparison of IMS Drag Predictions with 2D Nozzle Test Data (RC/RCM=0.12, A_9/A_{10}=0.2).

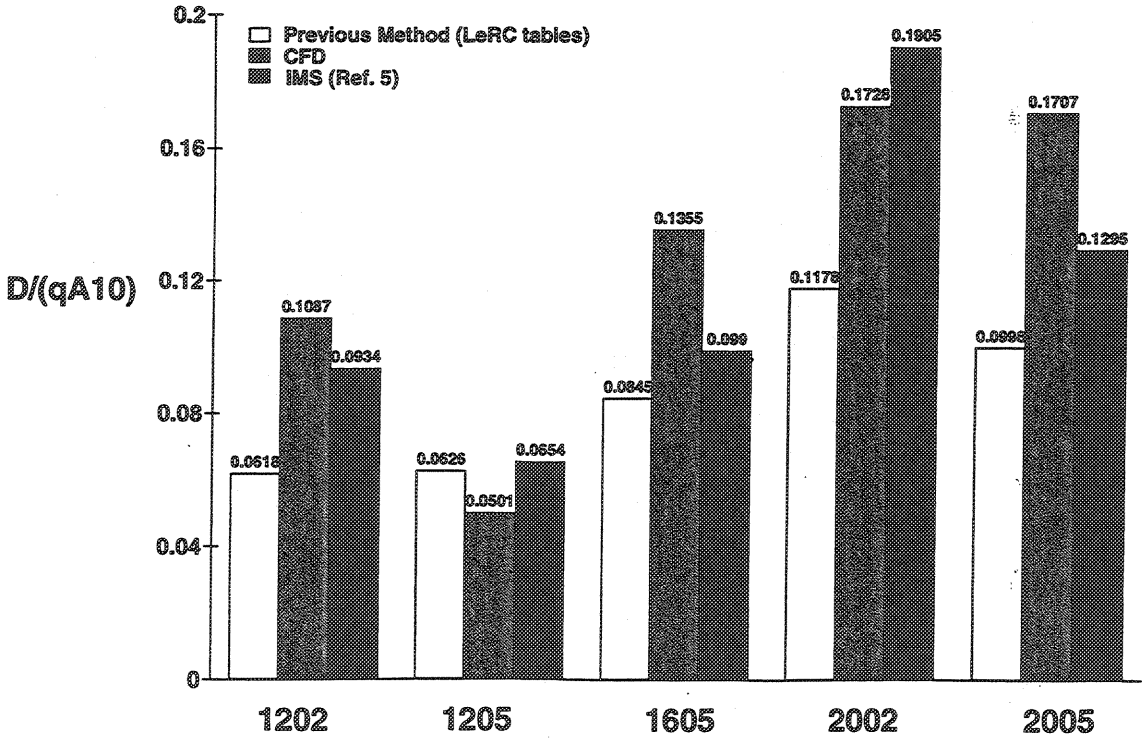

Figure 24. - Comparison of IMS, CFD and Previous Method Nozzle Boattail Drag Coefficient Predictions at M=0.95.

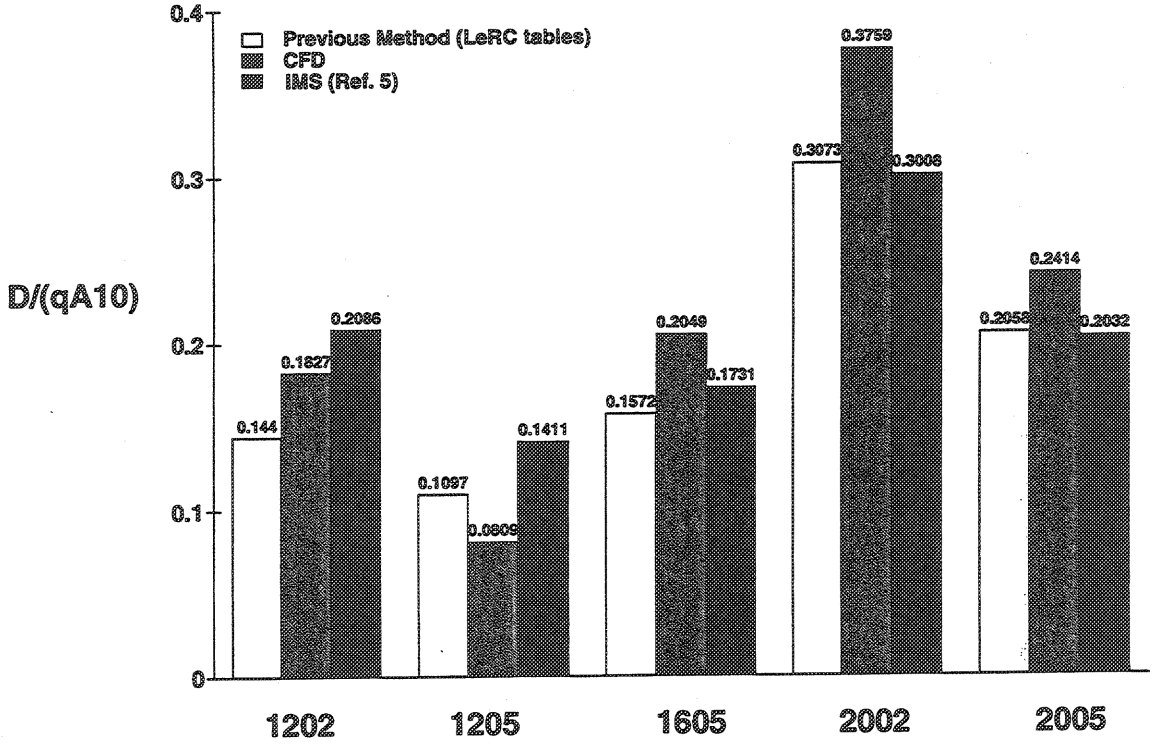

Figure 25. - Comparison of IMS, CFD and Previous Method Nozzle Boattail Drag Coefficient Predictions at M=1.1.

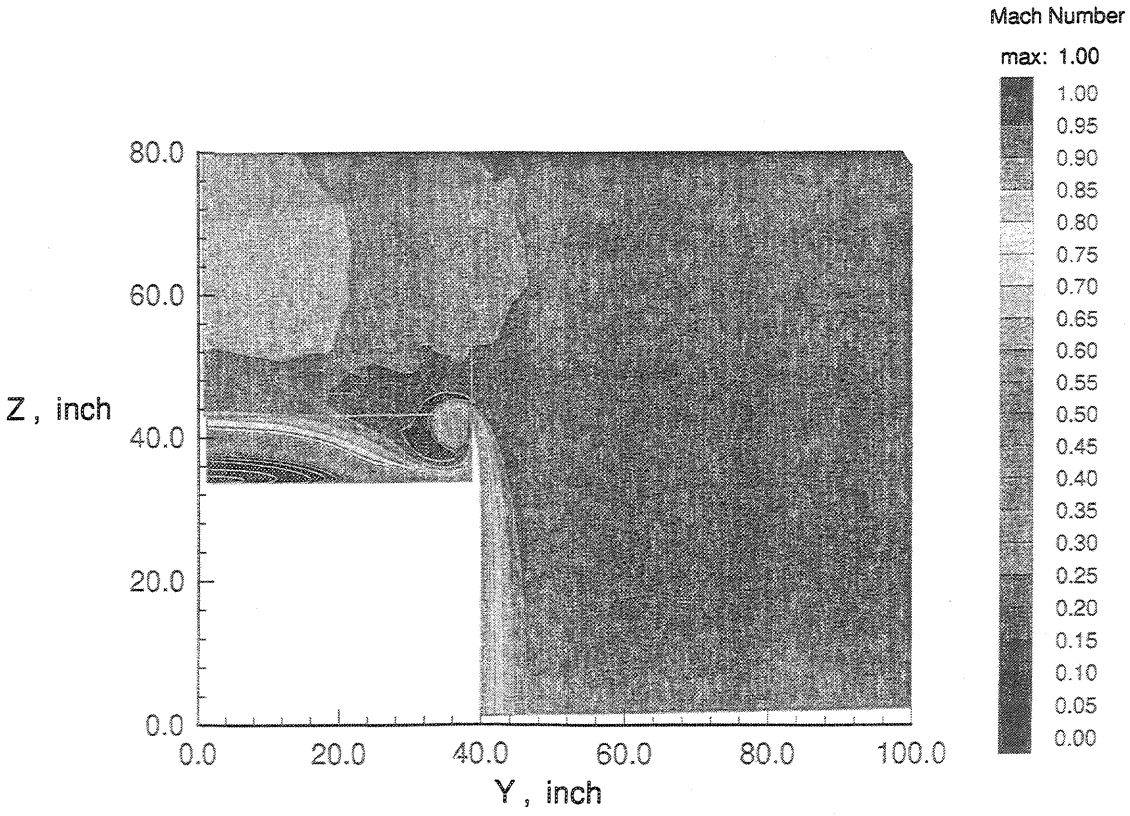

Figure 26. - Example of Mach Contour Flowfield Around DSM Nozzle Sidewall.

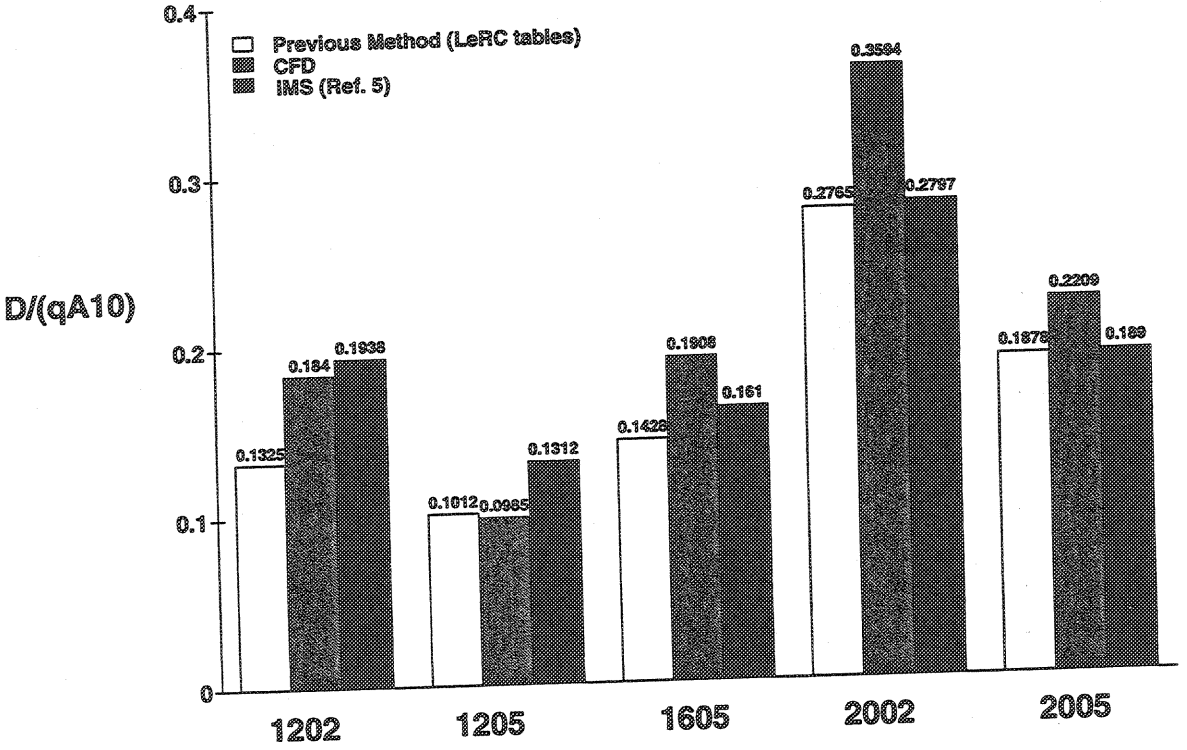

Figure 27. - Comparison of IMS, CFD and Previous Method Nozzle Boattail Drag Coefficient Predictions at M=1.2.

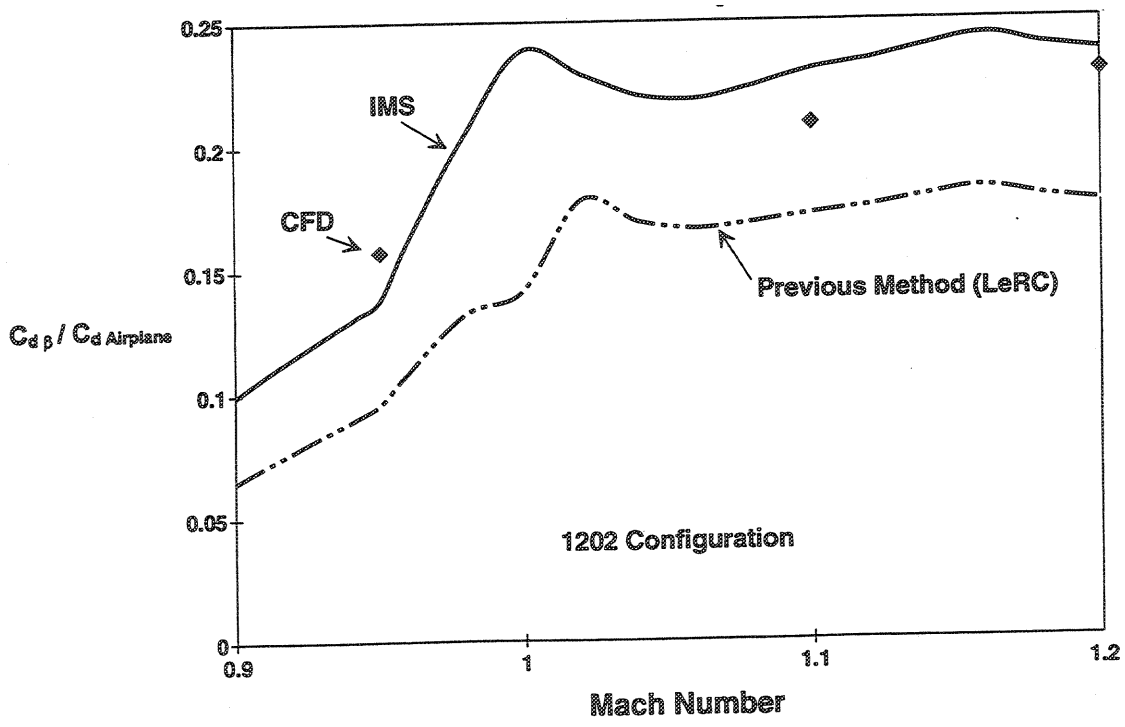

Figure 28. - Non-Dimensionalized Comparison of IMS, CFD and Previous Method Nozzle Boattail Drag Predictions with HSCT Total Airplane Drag for 1202 Configuration.

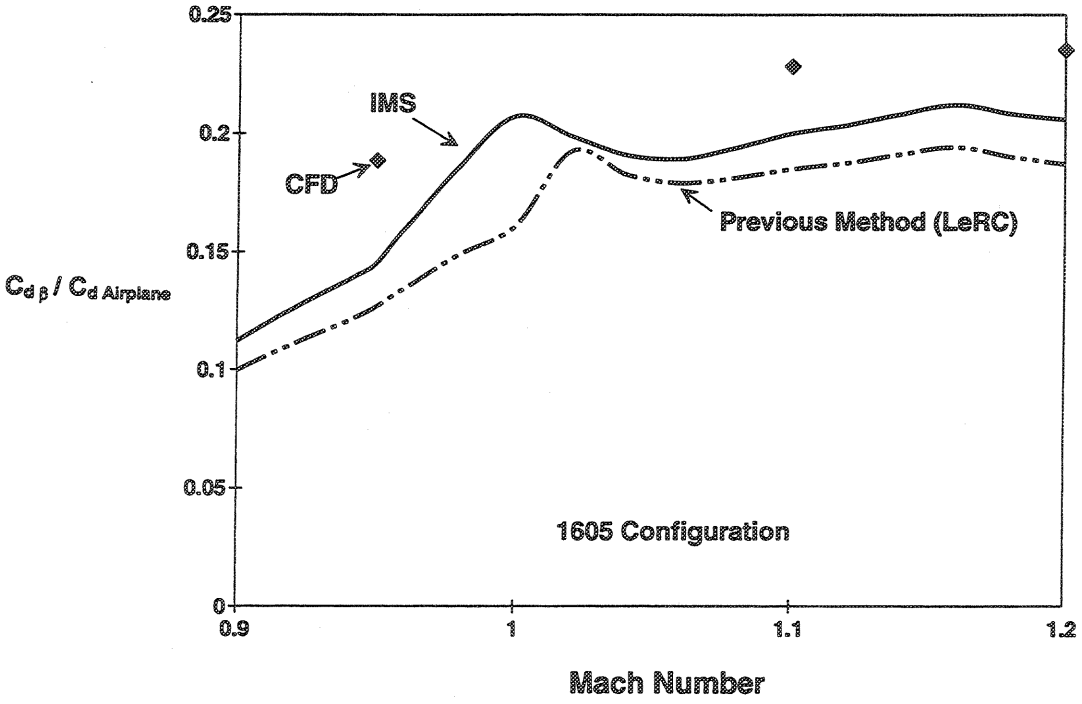

Figure 29. - Non-Dimensionalized Comparison of IMS, CFD and Previous Method Nozzle Boattail Drag Predictions with HSCT Total Airplane Drag for 1605 Configuration.

REPORT DOCUMENTATION PAGE

Form Approved
OMB No. 0704-0188

1. AGENCY USE ONLY (*Leave blank*)	2. REPORT DATE	3. REPORT TYPE AND DATES COVERED
	February 2005	Technical Memorandum

4. TITLE AND SUBTITLE

High Speed Civil Transport (HSCT) Isolated Nacelle Transonic Boattail Drag Study and Results Using Computational Fluid Dynamics (CFD)

5. FUNDING NUMBERS

WBS–22–714–09–46

6. AUTHOR(S)

Anthony C. Midea, Thomas Austin, S. Paul Pao, James R. DeBonis, and Mori Mani

7. PERFORMING ORGANIZATION NAME(S) AND ADDRESS(ES)

National Aeronautics and Space Administration
John H. Glenn Research Center at Lewis Field
Cleveland, Ohio 44135–3191

8. PERFORMING ORGANIZATION REPORT NUMBER

E–14892

9. SPONSORING/MONITORING AGENCY NAME(S) AND ADDRESS(ES)

National Aeronautics and Space Administration
Washington, DC 20546–0001

10. SPONSORING/MONITORING AGENCY REPORT NUMBER

NASA TM—2005-213384

11. SUPPLEMENTARY NOTES

This research was originally published internally as HSR025 in February 1996. Anthony C. Midea and James R. DeBonis, NASA Glenn Research Center; Thomas Austin, McDonnell Douglas Aerospace, Long Beach, California 90807; S. Paul Pao, NASA Langley Research Center; and Mori Mani, McDonnell Douglas Aerospace, St. Louis, Missouri 63166. Responsible person, Diane Chapman, Ultra-Efficient Engine Technology Program Office, NASA Glenn Research Center, organization code PA, 216–433–2309.

12a. DISTRIBUTION/AVAILABILITY STATEMENT

Unclassified - Unlimited
Subject Categories: 01, 02, 05, and 07 Distribution: Nonstandard

Available electronically at http://gltrs.grc.nasa.gov

This publication is available from the NASA Center for AeroSpace Information, 301–621–0390.

12b. DISTRIBUTION CODE

13. ABSTRACT ***(Maximum 200 words)***

Nozzle boattail drag is significant for the High Speed Civil Transport (HSCT) and can be as high as 25 percent of the overall propulsion system thrust at transonic conditions. Thus, nozzle boattail drag has the potential to create a thrust-drag pinch and can reduce HSCT aircraft aerodynamic efficiencies at transonic operating conditions. In order to accurately predict HSCT performance, it is imperative that nozzle boattail drag be accurately predicted. Previous methods to predict HSCT nozzle boattail drag were suspect in the transonic regime. In addition, previous prediction methods were unable to account for complex nozzle geometry and were not flexible enough for engine cycle trade studies. A computational fluid dynamics (CFD) effort was conducted by NASA and McDonnell Douglas to evaluate the magnitude and characteristics of HSCT nozzle boattail drag at transonic conditions. A team of engineers used various CFD codes and provided consistent, accurate boattail drag coefficient predictions for a family of HSCT nozzle configurations. The CFD results were incorporated into a nozzle drag database that encompassed the entire HSCT flight regime and provided the basis for an accurate and flexible prediction methodology.

14. SUBJECT TERMS	15. NUMBER OF PAGES
HSCT; Nacelle; Nozzle boattail drag	36
	16. PRICE CODE

17. SECURITY CLASSIFICATION OF REPORT	18. SECURITY CLASSIFICATION OF THIS PAGE	19. SECURITY CLASSIFICATION OF ABSTRACT	20. LIMITATION OF ABSTRACT
Unclassified	Unclassified	Unclassified	